


# Molecular Dynamics Simulations and Product Vibrational Spectral Analysis for the Reactions of NO<sub>2</sub> with 1-Ethyl-3-methylimidazolium Dicyanamide (EMIM<sup>+</sup>DCA<sup>-</sup>), 1-Butyl-3-methylimidazolium Dicyanamide (BMIM<sup>+</sup>DCA<sup>-</sup>), and 1-Allyl-3-methylimidazolium Dicyanamide (AMIM<sup>+</sup>DCA<sup>-</sup>)

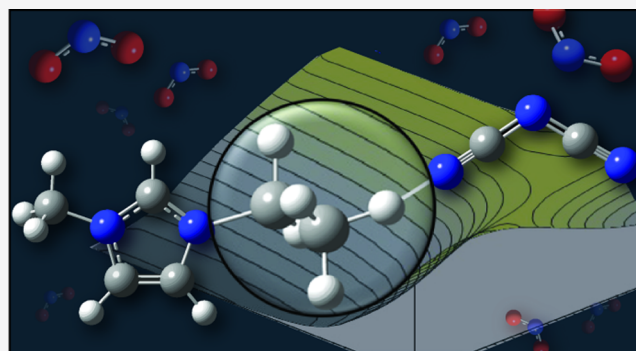
Jianbo Liu,\* Wenjing Zhou, Steven D. Chambreau, and Ghanshyam L. Vaghjiani

 Cite This: *J. Phys. Chem. B* 2020, 124, 4303–4325 Read Online

ACCESS |

 Metrics & More Article Recommendations Supporting Information

**ABSTRACT:** Direct dynamics trajectory simulations were carried out for the NO<sub>2</sub> oxidation of 1-ethyl-3-methylimidazolium dicyanamide (EMIM<sup>+</sup>DCA<sup>-</sup>), which were aimed at probing the nature of the primary and secondary reactions in the system. Guided by trajectory results, reaction coordinates and potential energy diagrams were mapped out for NO<sub>2</sub> with EMIM<sup>+</sup>DCA<sup>-</sup>, as well as with its analogues 1-butyl-3-methylimidazolium dicyanamide (BMIM<sup>+</sup>DCA<sup>-</sup>) and 1-allyl-3-methylimidazolium dicyanamide (AMIM<sup>+</sup>DCA<sup>-</sup>). Reactions of the dialkylimidazolium–dicyanamide (DCA) ionic liquids (ILs) are all initiated by proton transfer and/or alkyl abstraction between 1,3-dialkylimidazolium cations and DCA<sup>-</sup> anion, of which two exoergic pathways are particularly relevant to their oxidation activities. One pathway is the transfer of a H<sup>β</sup>-proton from the ethyl, butyl, or allyl group of the dialkylimidazolium cation to DCA<sup>-</sup> that results in the concomitant elimination of the corresponding alkyl as a neutral alkene, and the other pathway is the alkyl abstraction by DCA<sup>-</sup> via a second order nucleophilic substitution (S<sub>N</sub>2) mechanism. The intra-ion-pair reaction products, including [dialkylimidazolium<sup>+</sup> – H<sub>C2</sub><sup>+</sup>], alkylimidazole, alkene, alkyl-DCA, HDCA, and DCA<sup>-</sup>, react with NO<sub>2</sub> and favor the formation of nitrite (–ONO) complexes over nitro (–NO<sub>2</sub>) complexes, albeit the two complex structures have similar formation energies. The exoergic intra-ion-pair reactions in the dialkylimidazolium–DCA ILs account for their significantly higher oxidation activities over the previously reported 1-methyl-4-amino-1,2,4-triazolium dicyanamide [Liu, J.; et al. *J. Phys. Chem. B* 2019, 123, 2956–2970] and for the relatively higher reactivity of BMIM<sup>+</sup>DCA<sup>-</sup> vs AMIM<sup>+</sup>DCA<sup>-</sup> as BMIM<sup>+</sup> has a higher reaction path degeneracy for intra-ion-pair H<sup>β</sup>-proton transfer and its H<sup>β</sup>-transfer is more energetically favorable. To validate and directly compare our computational results with spectral measurements in the ILs, infrared and Raman spectra of BMIM<sup>+</sup>DCA<sup>-</sup> and AMIM<sup>+</sup>DCA<sup>-</sup> and their products with NO<sub>2</sub> were calculated using an ionic liquid solvation model. The simulated spectra reproduced all of the vibrational frequencies detected in the reactions of BMIM<sup>+</sup>DCA<sup>-</sup> and AMIM<sup>+</sup>DCA<sup>-</sup> IL droplets with NO<sub>2</sub> (as reported by Brotton et al. [*J. Phys. Chem. A* 2018, 122, 7351–7377] and Lucas et al. [*J. Phys. Chem. A* 2019, 123, 400–416]).



## 1. INTRODUCTION

Ionic liquids, ILs (defined as low melting salts that melt at or below 100 °C<sup>1</sup>), have become of interest within the aerospace research community as green propellant alternatives to the highly toxic, volatile, and sensitive hydrazine and its derivatives for rocket propulsion applications. The so-called energetic ILs in this context are composed of asymmetric N-rich heterocyclic cations and bulky anions.<sup>2</sup> They have extremely low vapor pressures (thus present low vapor toxicity and eliminate the hazard to human exposure), high thermal stability, and other favorable physical properties for storage, transportation, loading, and processing,<sup>1,3</sup> and they can react with an oxidizer such as N<sub>2</sub>O<sub>4</sub>/NO<sub>2</sub>, which is less toxic than hydrazine.<sup>4</sup> Since

dicyanamide (NCNCN<sup>-</sup>, abbreviated as DCA<sup>-</sup>)-based energetic ILs were reported as possible replacements for hydrazine in propellant formulations,<sup>5</sup> the design and synthesis of hypergolic ILs (i.e., those that spontaneously ignite when the energetic IL comes in contact with an oxidizer) have become an emerging

Received: March 13, 2020

Revised: May 1, 2020

Published: May 4, 2020



frontier in IL research. The designability of energetic ILs includes the choice of cation and anion within a single salt and the introduction of functional groups into the constituents. Studies have shown that cations affect the physicochemical properties of ILs, while anions are associated with hypergolicity and play a decisive role in the induction stage of ignition.<sup>1</sup> The DCA<sup>-</sup> anions were utilized for hypergolic ILs because of their high nitrogen content and low viscosity (which facilitates the rapid mixing of ILs with an oxidizer and makes initiation and combustion faster),<sup>5</sup> and the 1,3-dialkylimidazolium cations were chosen due to their high energy density, high stability, and structural adjustability through the control of alkyl substituents.<sup>1</sup>

A commonly accepted ignition mechanism between hypergolic ILs and an oxidizer involves two stages: a low-temperature preignition stage during which exothermic redox reactions lead to the formation of gaseous transient species and release of heat, followed by a stage in which the system temperature reaches the kindling point of the highly inflammable gaseous species leading to ignition and subsequent combustion to occur.<sup>1,6</sup> Therefore, understanding IL thermal stabilities, their reaction mechanisms, and pathways leading to ignition and their associated reaction dynamics and reaction kinetics is of utmost importance in predicting the performance of hypergolic ILs and in optimizing the design of propulsion systems that use ILs. We previously reported photoionization mass spectrometric and infrared spectroscopic measurements<sup>7</sup> and molecular dynamics simulations<sup>8</sup> of the thermal decomposition of 1-ethyl-3-methylimidazolium dicyanamide (EMIM<sup>+</sup>DCA<sup>-</sup>) and 1-ethyl-2,3-dimethylimidazolium dicyanamide (EMMIM<sup>+</sup>DCA<sup>-</sup>). The combination of experimental and theoretical approaches allowed us to determine the decomposition products, branching ratios, and underlying reaction kinetics and reaction dynamics of alkylimidazolium–DCA ILs.

Recently, Kasier and co-workers<sup>9</sup> reported the reaction of NO<sub>2</sub> with levitated droplets of 1-methyl-4-amino-1,2,4-triazolium dicyanamide (MAT<sup>+</sup>DCA<sup>-</sup>) using infrared and Raman spectroscopic probes, in which many new vibrational bands were observed for the oxidation products. Inspired by their results, we utilized direct dynamics trajectory simulations to probe the most likely reaction pathways and products of MAT<sup>+</sup>DCA<sup>-</sup> + NO<sub>2</sub>.<sup>10</sup> Analysis of the trajectory outcomes combined with exploration of the reaction coordinates and reaction potential energy (PE) diagrams helped us identify the primary and secondary reactions in this system. More recently, Kasier and co-workers reported similar spectroscopic investigations of the reactions of NO<sub>2</sub> with levitated droplets of 1-butyl-3-methylimidazolium dicyanamide (BMIM<sup>+</sup>DCA<sup>-</sup>)<sup>11</sup> and 1-allyl-3-methylimidazolium dicyanamide (AMIM<sup>+</sup>DCA<sup>-</sup>).<sup>12</sup> Following their new experiments, the present work extends our theoretical investigations to the NO<sub>2</sub> reactions with EMIM<sup>+</sup>DCA<sup>-</sup>, BMIM<sup>+</sup>DCA<sup>-</sup>, and AMIM<sup>+</sup>DCA<sup>-</sup> to ascertain the cation structural complexity effects.

## 2. APPROACHES FOR DIRECT DYNAMICS SIMULATIONS AND REACTION COORDINATE CALCULATIONS

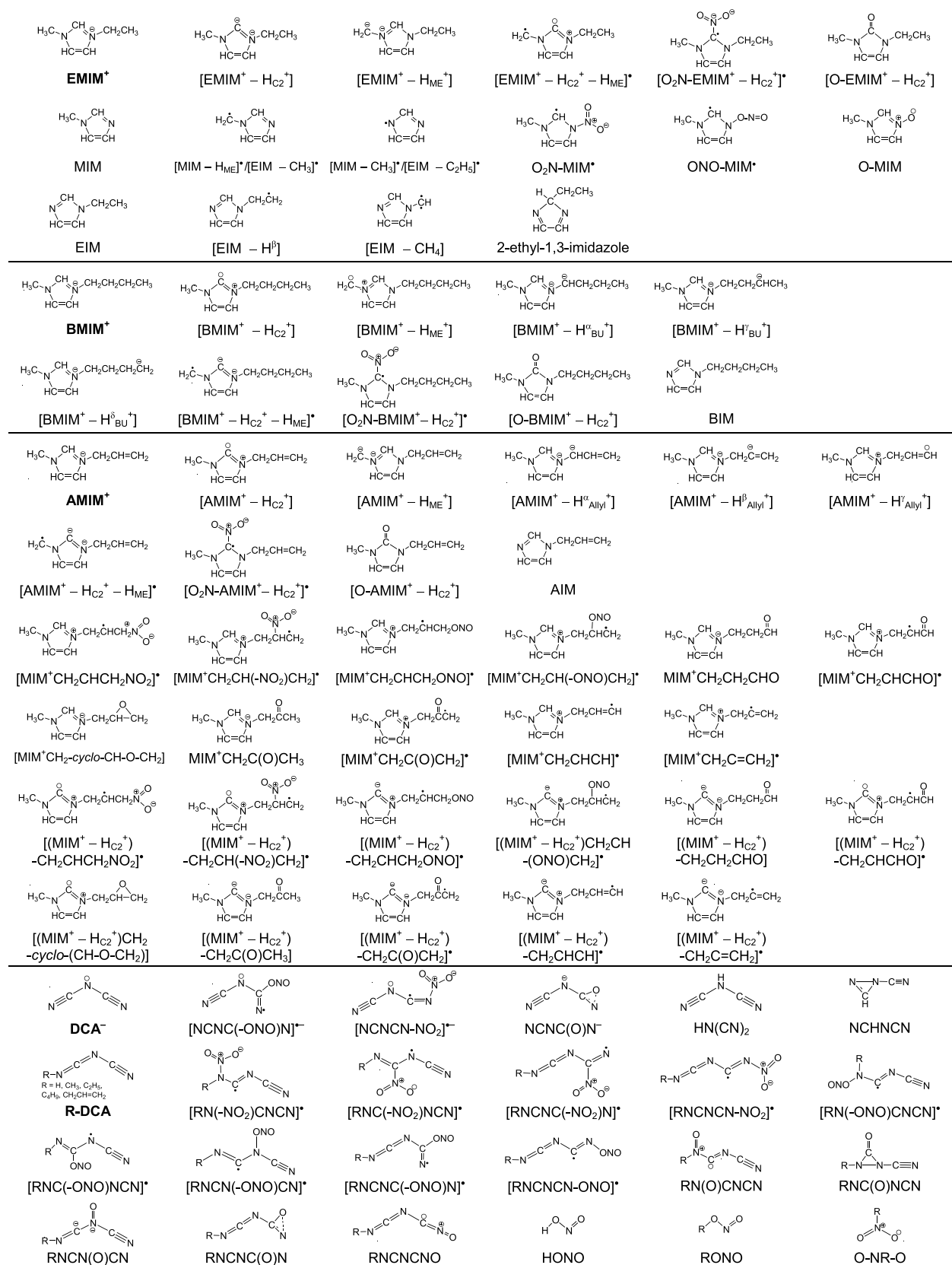
The heat of combustion of energetic ILs is large by virtue of their high heat of formation. Once combustion occurs upon heating, the resulting oxidation and decomposition of ILs can be vigorous, and these reactions may go to completion within a few nanoseconds. These features of energetic ILs make it a challenge to experimentally detect, in situ, all of the generated transient species. Computational modeling offers an alternative to

experimental measurements for testing and ascertaining the possibility of various mechanisms in IL ignition. A complication in IL dissociation and oxidation is that these processes are often controlled by dynamics (particularly at high temperatures) and do not necessarily follow the minimum energy pathways.<sup>10</sup> Furthermore, reactions may be autocatalytic,<sup>13</sup> and non-statistical distributions among multiple product channels may arise from direct collisions or non-Rice–Ramsperger–Kassel–Marcus (RRKM)<sup>14</sup> unimolecular processes. Accordingly, the cognitive use of chemical intuition may be inadequate to predict IL reactions. As such, an appropriate approach for examining IL reactions would be to use direct dynamics simulations and to energize reactants under specific conditions.<sup>15–24</sup> Direct dynamics simulations do not require the use of analytical potential energy surfaces (PESs); instead, energies, force constants, and Hessians are calculated “on the fly”. Accordingly, this method becomes computationally attractive when the dimensionality of a system increases. The direct dynamics trajectories explore multiple minima in the conformational landscape and on the reaction PES. The motions of molecules are followed in time, wherein the molecules show what the preferred pathways and product structures are. A discovery element of the simulations is the ability to identify new unexpected reactions and energy dissipation pathways for energetic ILs<sup>21,23–25</sup> and to locate reaction activation barriers and rate-limiting steps by following the variations in the potential energy and bond lengths along the trajectories.<sup>21,22,26</sup>

In the present work, we first used EMIM<sup>+</sup>DCA<sup>-</sup> + NO<sub>2</sub> as a model system to mimic the general features of the primary and secondary reactions of 1,3-dialkylimidazolium–DCA with NO<sub>2</sub>. In light of the trajectory findings of EMIM<sup>+</sup>DCA<sup>-</sup> + NO<sub>2</sub>, the reaction coordinates and the associated potential energy diagrams for the decomposition of EMIM<sup>+</sup>DCA<sup>-</sup> and for the reactions of its primary products with NO<sub>2</sub> were mapped out using density functional theory (DFT). The important reaction pathways identified in EMIM<sup>+</sup>DCA<sup>-</sup> + NO<sub>2</sub> were then inferred to be occurring in the more extended systems of BMIM<sup>+</sup>DCA<sup>-</sup> + NO<sub>2</sub> and AMIM<sup>+</sup>DCA<sup>-</sup> + NO<sub>2</sub>, whose feasibilities were also evaluated using the DFT calculations. Finally, to validate the computational results, infrared and Raman spectra of the theoretically predicted NO<sub>2</sub>-oxidation products of BMIM<sup>+</sup>DCA<sup>-</sup> and AMIM<sup>+</sup>DCA<sup>-</sup> were calculated and compared with Kasier et al.’s measurements for the same systems.<sup>11,12</sup>

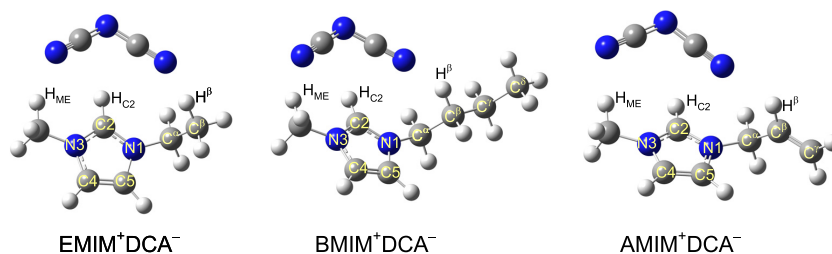
Methodologies of direct dynamics simulations are provided in the Supporting Information. In brief, initial conditions for trajectories were set up using VENUS,<sup>27,28</sup> and the Hessian-based predictor–corrector algorithm,<sup>20</sup> implemented in Gaussian 09,<sup>29</sup> was used to integrate the trajectories. The B3LYP/6-31G(d) level of theory was used for the simulations as this functional was satisfactory in calculating the energetics of dialkylimidazolium<sup>30–34</sup> and triazolium-based<sup>35</sup> ILs, the infrared and Raman spectra of dialkylimidazolium-ILs,<sup>36–40</sup> and the dynamics of EMIM<sup>+</sup>DCA<sup>-</sup>,<sup>8</sup> EMMIM<sup>+</sup>DCA<sup>-</sup>,<sup>8</sup> and MAT<sup>+</sup>DCA<sup>-</sup>.<sup>10</sup> Trajectories were propagated using a quadratically convergent self-consistent field (SCF) procedure<sup>29,41</sup> with a step size of 0.25 amu<sup>1/2</sup> b. In a previous work,<sup>10</sup> we had examined the explicit IL solvent effects on the reaction of [MAT<sup>+</sup> – H<sub>CS</sub><sup>+</sup>] + NO<sub>2</sub> by running the same trajectories for the gas-phase and the condensed-phase ILs. The two sets of trajectories followed the same reaction pathways, with the only difference being a small decrease in the product recoil energy in the ILs. Since the trajectory results showed little differences in

Scheme 1. ChemDraw Structures of Reactant Ions, Intermediates, and Products



the gas-phase vs the condensed-phase IIs, and since the gas-phase computation was much faster than that of the condensed phase, all trajectories in the present work were simulated in the gas phase. Trajectory calculations were completed on a Linux

computer cluster. gOpenMol<sup>42</sup> was used for trajectory visualization. Sorting of reaction pathways and analysis of trajectory ensembles were carried out with custom programs written for these purposes.

Scheme 2. Optimized Structures of EMIM<sup>+</sup>DCA<sup>-</sup>, BMIM<sup>+</sup>DCA<sup>-</sup>, and AMIM<sup>+</sup>DCA<sup>-</sup> with the Atom-Numbering SchemesTable 1. Trajectory Reaction Probabilities (%) for EMIM<sup>+</sup>DCA<sup>-</sup> + NO<sub>2</sub> at Various Conditions<sup>a</sup>

temperature (K)	1000	2000	3000	4000	5000	
$E_{\text{col}}$ (eV)	0.1	0.1	0.1	0.1	without NO <sub>2</sub> <sup>b</sup>	
PT1: [EMIM <sup>+</sup> - H <sub>C2</sub> <sup>+</sup> ] + HDCA	0	14 ± 3	23 ± 4	13 ± 3	31 ± 5	24 ± 4
PT2: [EMIM <sup>+</sup> - H <sub>C2</sub> <sup>+</sup> ] + NCHNCN	0	0	4 ± 2	2 ± 1	0	0
PT3: [EMIM <sup>+</sup> - H <sub>C2</sub> <sup>+</sup> ] + HN(CN) <sub>2</sub>	0	2 ± 1	0	3 ± 2	0	6 ± 2
PT4: MIM + C <sub>2</sub> H <sub>4</sub> + HDCA	0	0	0	5 ± 2	0	3 ± 2
ethyl elimination: MIM <sup>+</sup> + C <sub>2</sub> H <sub>5</sub> + DCA <sup>-</sup>	0	0	7 ± 3	31 ± 5	0	27 ± 4
methyl elimination: EIM <sup>+</sup> + CH <sub>3</sub> + DCA <sup>-</sup>	0	0	11 ± 3	11 ± 3	0	6 ± 2
ethyl abstraction: MIM + C <sub>2</sub> H <sub>5</sub> DCA	0	0	2 ± 1	3 ± 2	30 ± 5	0
methyl abstraction: EIM + CH <sub>3</sub> DCA	0	0	2 ± 1	2 ± 1	10 ± 3	0
ion-pair breaking	0	14 ± 3	42 ± 5	60 ± 5	93 ± 3	33 ± 5
fragmentation of EMIM <sup>+</sup>	0	0	2 ± 1	9 ± 3	8 ± 3	33 ± 5
fragmentation of DCA <sup>-</sup>	0	4 ± 2	11 ± 3	20 ± 4	12 ± 3	36 ± 8

<sup>a</sup>Percent probabilities and uncertainties were calculated on the basis of 100 trajectories for each condition. PT, ion-pair breaking, and fragmentation may all happen in a single trajectory, occurring either simultaneously or sequentially. <sup>b</sup>Data from ref 8.

To construct reaction coordinates for the trajectory-predicted pathways, structures of the reactants and of the corresponding reaction intermediates, transition states (TSs) and products were recalculated at the B3LYP/6-311++G(d,p) level of theory using Gaussian 09<sup>29</sup> or Gaussian 16.<sup>43</sup> Structures of the TSs were optimized by using a number of high potential energy, barrier-like geometries identified in the reactive trajectories as starting points. The Cartesian coordinates for all of the species along the calculated reaction coordinates are provided in the Supporting Information. ChemDraw structures of all reactants and products are depicted in Scheme 1. Reaction enthalpies ( $\Delta H$ ) and changes in free energy ( $\Delta G$ ) were evaluated at 298 K, for which the zero-point energies (ZPEs) were scaled by a factor of 0.981.<sup>44</sup>

The infrared and Raman spectra of reactants and products were simulated in a condensed-phase IL environment so that they could be directly compared with the experimental measurements of the same IL reactions. To this end, the structures of the corresponding reactants and products were re-optimized using the parameterized self-consistent reaction field (SCRFF) which involves the solvation model based on density (SMD)<sup>45</sup> (also known as the generic ionic liquid solvation model, SMD-GIL)<sup>46</sup> with appropriate solvent parameters. Due to convergence difficulties encountered for some of the IL structures when performing the SMD-GIL-coupled B3LYP calculations, the SMD-GIL//M06/6-311++G(d,p) method<sup>47</sup> was instead adopted for spectral simulations. The latter method has been successfully used in the spectral analysis for the reaction of MAT<sup>+</sup>DCA<sup>-</sup> IL droplet with NO<sub>2</sub>.<sup>9</sup>

### 3. REACTION DYNAMICS, REACTION COORDINATES, AND REACTION ENERGETICS FOR EMIM<sup>+</sup>DCA<sup>-</sup> + NO<sub>2</sub>

**3.1. Primary Reactions.** Prior to trajectory simulations and reaction coordinate calculations, conformations of EMIM<sup>+</sup>DCA<sup>-</sup>, BMIM<sup>+</sup>DCA<sup>-</sup>, and AMIM<sup>+</sup>DCA<sup>-</sup> were optimized at the B3LYP/6-311++G(d,p) level of theory to ensure that their global minima were used as starting geometries in the computational modeling. Scheme 2 illustrates the lowest-energy structures of the three ILs together with the atom-numbering scheme used. It is to be noted that the ILs are vigorously excited in the trajectories as a result of excitations due to the high temperatures and due to the collisions with NO<sub>2</sub>. Consequently, the simulations explore all energetically accessible structures during trajectory propagation, and all of the various reactant conformers are able to form and contribute to the trajectory outcomes, despite the fact that all of the trajectories are being initiated from a global minimum structure. This consequence results from the inherent nature of direct dynamics, which incorporates all of the various energy contents of the reacting species and explores reaction pathways in an unbiased manner.

We first simulated the reaction of an intact ion pair of EMIM<sup>+</sup>DCA<sup>-</sup> with NO<sub>2</sub> at a 0.1 eV center-of-mass (CM) collision energy ( $E_{\text{col}}$ ) and in the high-temperature range from 1000 to 5000 K. High temperatures were used to enhance the reaction probability within the trajectory integration time (of ~3 ps). These temperatures are much higher than the decomposition temperature in a typical experimental pyrolysis reactor. As a result, some trajectories may find reaction pathways with activation barriers too high to be of relevance to the ignition process under realistic experimental temperatures. The point is that with enough trajectories, all of the reaction pathways can be identified, including those that control reactions under the

conditions of interest. Once these pathways are found, their reaction coordinates and potential energy diagrams are calculated with the relevant TSs and intermediates, and one only needs to consider those that are able to contribute significantly to the kinetics of ignition.

Hundred trajectories were calculated for each of the five initial conditions we chose. Trajectory results are summarized in Table 1, where the first column describes reaction pathways. Note that multiple reaction pathways may occur in the same trajectory, thereby causing the sum of reaction probabilities to be >100% at some temperatures. Statistical uncertainties of the reaction probabilities were calculated on the basis of the number of total trajectories and the number of reactive trajectories for individual pathways. No direct reaction was observed between  $\text{EMIM}^+\text{DCA}^-$  and  $\text{NO}_2$  at any of the simulation temperatures. The trajectories at 1000 K can all be characterized as direct, nonreactive collisions. Ion-pair breaking started to emerge at 2000 K and increased with temperature. Fragmentation of  $\text{EMIM}^+$  and  $\text{DCA}^-$  moieties was observed during ion-pair dissociation (either simultaneously or sequentially), and  $\text{DCA}^-$  was more prone to decomposition than  $\text{EMIM}^+$ . Besides ion-pair dissociation and ion decomposition, the other trajectory-predicted intra-ion-pair reactions are as follows.

**3.1.1. Proton Transfer (PT).** The most common outcome of  $\text{EMIM}^+\text{DCA}^- + \text{NO}_2$  collisions corresponded to intra-ion-pair PT from the C2 of  $\text{EMIM}^+$  to a terminal N of  $\text{DCA}^-$ , forming  $[\text{EMIM}^+ - \text{H}_{\text{C}_2}] + \text{HDCA}$  (referred to as PT1). PT1 represents a probability of 13–24% at all temperatures above 1000 K. Some trajectories underwent reversible PT, and these trajectories were counted as nonreactive as long as the trajectories returned to their starting structures. The second intra-ion-pair PT pathway (PT2, 2–4% at 3000–4000 K) transfers the proton from the C2 of  $\text{EMIM}^+$  to a C atom of  $\text{DCA}^-$ , forming  $[\text{EMIM}^+ - \text{H}_{\text{C}_2}] + \text{NCHNCN}$ . The third intra-ion-pair PT pathway (PT3, 3–6% at 4000–5000 K) transfers the proton from the C2 of  $\text{EMIM}^+$  to the central N of  $\text{DCA}^-$ , forming  $[\text{EMIM}^+ - \text{H}_{\text{C}_2}] + \text{HN}(\text{CN})_2$ .

The last yet mechanistically most interesting intra-ion-pair PT involves the transfer of a  $\text{H}^\beta$ -proton from the  $\text{EMIM}^+$  ethyl to a terminal N of  $\text{DCA}^-$ , which triggers the dissociation of the  $\text{N1}$ -ethyl bond, producing methylimidazole ( $\text{MIM}$ ) +  $\text{C}_2\text{H}_4$  +  $\text{HDCA}$  (referred to as PT4). PT4 was observed at 4000 K and above, with a probability of 3–5%. Figure 1 demonstrates a representative PT4 trajectory. The top frame of the figure plots the changes in the system potential energy, PE (left axis), and the center-of-mass, CM, distance (right axis) between  $\text{EMIM}^+\text{DCA}^-$  and  $\text{NO}_2$  throughout the trajectory. The oscillations in the PE reflect the vibrations of reactants/products, including their ZPEs. The collision between  $\text{EMIM}^+\text{DCA}^-$  and  $\text{NO}_2$  is direct as evidenced by a single turning point of the CM distance (around 410 fs) at which the collision occurred. The bottom frame shows the changes in various bond lengths participating in the reaction. In this trajectory, the  $\text{H}^\beta$ -proton had a brief transfer between  $\text{C}^\beta$  and  $\text{DCA}^-$  from 50 to 110 fs. PT4 happened at 460 fs (slightly after the collision point), which was indicated by the dissociation of  $r\text{N1}-\text{C}_2\text{H}_5$  and  $r\text{C}^\beta-\text{H}^\beta$  and the concurrent formation of  $r\text{H}^\beta-\text{DCA}$ . Note that PT4 could also occur before the collision as we observed in the other PT4 trajectories.

**3.1.2. Direct Alkyl Elimination.** Another major group of reactive trajectories involves the elimination of an alkyl group from  $\text{EMIM}^+\text{DCA}^-$  that accompanied ion-pair breaking, producing methylimidazolium cation ( $\text{MIM}^+$ ) and  $\text{C}_2\text{H}_5 + \text{DCA}^-$  (accounting for 7–31% of the trajectories at 3000–5000

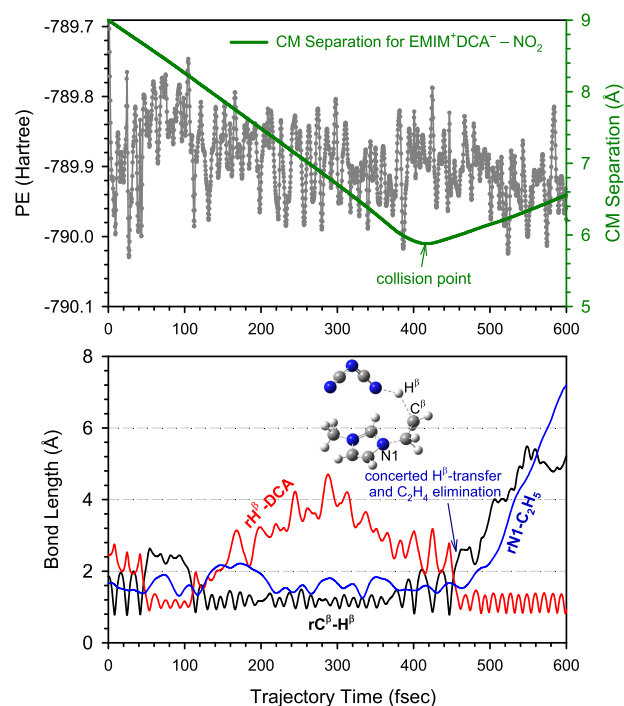


**Figure 1.** Representative trajectory of PT4 for  $\text{EMIM}^+\text{DCA}^-$  during its collision with  $\text{NO}_2$ , simulated at 4000 K and 0.1 eV collision energy. (Top) The variations in the PE and in the CM distance between the collision partners, and (bottom) the variations of various bond lengths participating in the reaction. Snapshot shows concerted  $\text{H}^\beta$ -transfer and ethylene elimination. Video of the trajectory is available in the Supporting Information.

K) or ethylimidazolium cation ( $\text{EIM}^+$ ) and  $\text{CH}_3 + \text{DCA}^-$  (6–11% at 3000–5000 K).

**3.1.3. Alkyl Abstraction.** Different from direct alkyl elimination, this group of trajectories has an alkyl group of  $\text{EMIM}^+$  abstracted by a terminal N of  $\text{DCA}^-$ , producing a pair of neutral products methylimidazole ( $\text{MIM}$ ) +  $\text{C}_2\text{H}_5\text{DCA}$  or ethylimidazole ( $\text{EIM}$ ) +  $\text{CH}_3\text{DCA}$ . Abstraction may be mediated by a first-order nucleophilic substitution ( $\text{S}_{\text{N}}1$ ) or second-order nucleophilic substitution ( $\text{S}_{\text{N}}2$ ) mechanism, and the latter is energetically more favorable<sup>8,48</sup> (vide infra). In  $\text{S}_{\text{N}}2$  ethyl abstraction, the departure of the imidazole ring occurs simultaneously with the backside attack by  $\text{DCA}^-$  and the  $\text{C}^\alpha\text{H}_2$  group becomes planar during the abstraction. Alkyl abstraction only happens with a terminal N but not with the central N of  $\text{DCA}^-$ , presumably because the barrier leading to the formation of a terminally alkylated DCA is lower than that for a centrally alkylated DCA.<sup>30</sup>

In a previous work,<sup>8</sup> we simulated thermal decomposition of single  $\text{EMIM}^+\text{DCA}^-$  at 4000 K using the B3LYP/6-31G(d) level of theory. The results are included in Table 1 for comparison.  $\text{EMIM}^+\text{DCA}^-$  has shown significant ion-pair dissociation and ion decomposition both with and without  $\text{NO}_2$ . PT1 is important under both conditions (and becomes the only PT pathway in the thermal trajectories). A major difference between the collision trajectories of  $\text{EMIM}^+\text{DCA}^- + \text{NO}_2$  and the thermal trajectories of  $\text{EMIM}^+\text{DCA}^-$  concerns alkyl elimination and abstraction. The probabilities of methyl and ethyl abstractions in the thermal trajectories are an order of magnitude higher than in the collision trajectories (see the 4000 K column), whereas the probabilities of methyl and ethyl elimination in the thermal trajectories drop to zero. The

different reaction probabilities in the thermal decomposition of  $\text{EMIM}^+\text{DCA}^-$  vs in the collisions of  $\text{EMIM}^+\text{DCA}^- + \text{NO}_2$  can be rationalized as follows: in the collision trajectories, part of collision energy was transferred to product recoil energy; as a consequence, the ions have acquired sufficient momenta to depart from each other, and the ion-pair lifetime was too short to initiate a complex-mediated  $\text{S}_{\text{N}}2$  abstraction.

As aforementioned, the trajectory temperatures were higher than the experimental temperature. To identify the most relevant pathways under experimental conditions, the reaction coordinates and reaction energetics for all of the trajectory-predicted reactions were calculated at the B3LYP/6-311++G(d,p) level of theory, results of which are summarized in Figure 2. Figure 2 gives both reaction  $\Delta H$  (298 K) and  $\Delta G$  (298 K) for individual TSs and products, and their structures are depicted in Scheme 1 and in the Supporting Information.

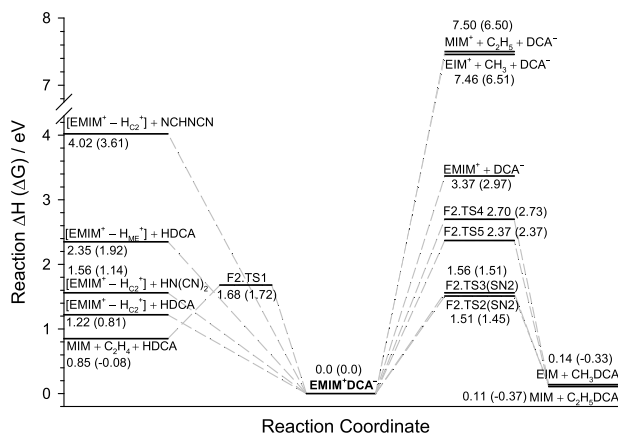


**Figure 2.** Reaction coordinates for the decomposition of  $\text{EMIM}^+\text{DCA}^-$ . Reaction  $\Delta H$  (eV) and  $\Delta G$  (eV, in parentheses) were calculated at the B3LYP/6-311++G(d,p) level of theory, including thermal corrections at 298 K. Cartesian coordinates of stable structures and TSs are provided in the Supporting Information.

Analysis of the collision trajectories of  $\text{EMIM}^+\text{DCA}^-$  with  $\text{NO}_2$ , the thermal activation trajectories of  $\text{EMIM}^+\text{DCA}^-$ , and the reaction potential energy diagram of  $\text{EMIM}^+\text{DCA}^-$  decomposition has led to the following points: (1) PT1 and PT4 are the two most favorable intra-ion-pair reactions, yielding stable products  $[\text{EMIM}^+ - \text{H}_{\text{C}_2}^+] + \text{HDCA}$  and  $\text{MIM} + \text{C}_2\text{H}_4 + \text{HDCA}$ . PT1 has no reverse barrier, and the reaction initiates at the thermodynamic threshold. PT4 has a negative change in free energy and thus releases heat in the reaction. (2) Another energetically and dynamically favorable process is  $\text{S}_{\text{N}}2$  alkyl abstraction, producing  $\text{MIM} + \text{C}_2\text{H}_5\text{DCA}$  and  $\text{EIM} + \text{CH}_3\text{DCA}$ . These findings have thus motivated us to examine the reactions of  $\text{NO}_2$  with the primary products  $[\text{EMIM}^+ - \text{H}_{\text{C}_2}^+]$ ,  $\text{MIM}$ ,  $\text{EIM}$ ,  $\text{HDCA}$ ,  $\text{CH}_3\text{DCA}$ ,  $\text{C}_2\text{H}_5\text{DCA}$ , and  $\text{C}_2\text{H}_4$ .

**3.2.  $[\text{EMIM}^+ - \text{H}_{\text{C}_2}^+] + \text{NO}_2$ .** The bimolecular collisions were simulated at temperatures from 1000 to 4000 K and  $E_{\text{col}}$  of 0.1 and 0.5 eV. No reaction was observed at 1000 K. Reactions at higher temperatures can be grouped into three types, as listed in Table 2. The first group leads to the formation of an aromatic nitro radical complex  $[\text{O}_2\text{N} - \text{EMIM}^+ - \text{H}_{\text{C}_2}^+]^{\bullet}$  (as  $\text{NO}_2$  is a molecular radical), wherein the N of  $\text{NO}_2$  is bonded to the C2 of  $[\text{EMIM}^+ - \text{H}_{\text{C}_2}^+]$ . All of the  $[\text{O}_2\text{N} - \text{EMIM}^+ - \text{H}_{\text{C}_2}^+]^{\bullet}$  complexes decayed back to reactants before the end of the trajectories. The second group is featured by the abstraction of a  $\text{NO}_2$  oxygen atom by the C2 of  $[\text{EMIM}^+ - \text{H}_{\text{C}_2}^+]$ , producing 1-ethyl-3-methyl-1,3-dihydro-2H-imidazole-2-one ( $[\text{O} - \text{EMIM}^+ - \text{H}_{\text{C}_2}^+] + \text{NO}$ ). The third group represents a hydrogen transfer (HT) from the methyl of  $[\text{EMIM}^+ - \text{H}_{\text{C}_2}^+]$  to  $\text{NO}_2$ , producing  $[\text{EMIM}^+ - \text{H}_{\text{C}_2}^+ - \text{H}_{\text{ME}}]^{\bullet}$  and nitrous acid  $\text{HONO}$ . In addition, the elimination of  $\text{H}_2$ ,  $\text{CH}_3$ , or  $\text{C}_2\text{H}_5$  from  $[\text{EMIM}^+ - \text{H}_{\text{C}_2}^+]$  was observed at 3000–4000 K.

Reaction coordinates for the three reaction pathways are shown in Figure 3. Reaction is initiated by a precursor complex

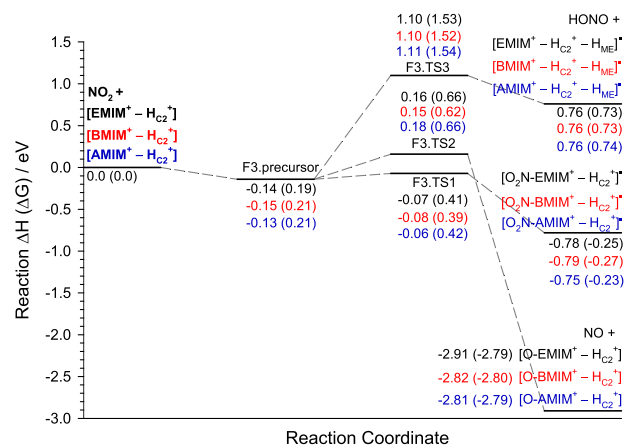


**Figure 3.** Reaction coordinates for  $\text{NO}_2$  with  $[\text{EMIM}^+ - \text{H}_{\text{C}_2}^+]$  (indicated in black),  $[\text{BMIM}^+ - \text{H}_{\text{C}_2}^+]$  (red), and  $[\text{AMIM}^+ - \text{H}_{\text{C}_2}^+]$  (blue). Reaction  $\Delta H$  (eV) and  $\Delta G$  (eV, in parentheses) were calculated at the B3LYP/6-311++G(d,p) level of theory, including thermal corrections at 298 K. Cartesian coordinates of stable structures and TSs are provided in the Supporting Information.

formed by the electrostatic binding of 0.14 eV, from which three TSs lead the system into three different product channels. The fact that the binding energy of  $[\text{O}_2\text{N} - \text{EMIM}^+ - \text{H}_{\text{C}_2}^+]^{\bullet}$  is only 0.78 eV and that it was short-lived in the trajectories implies that this complex is better described as an electrostatically bound entity rather than a covalent one. As a consequence, the most likely products of  $[\text{EMIM}^+ - \text{H}_{\text{C}_2}^+]$  with  $\text{NO}_2$  are  $[\text{O} - \text{EMIM}^+ - \text{H}_{\text{C}_2}^+] + \text{NO}$  followed by  $[\text{EMIM}^+ - \text{H}_{\text{C}_2}^+ - \text{H}_{\text{ME}}]^{\bullet} + \text{HONO}$ .

**3.3. Reactions of  $\text{NO}_2$  with MIM and EIM.** A batch of 100 collision trajectories each was calculated for both  $\text{MIM} + \text{NO}_2$

**Table 2. Trajectory Reaction Probabilities (%) for  $[\text{EMIM}^+ - \text{H}_{\text{C}_2}^+] + \text{NO}_2$  at Various Conditions<sup>a</sup>**

temperature (K)	1000		2000		3000		4000	
	$E_{\text{col}}$ (eV)		$E_{\text{col}}$ (eV)		$E_{\text{col}}$ (eV)		$E_{\text{col}}$ (eV)	
short-lived $[\text{O}_2\text{N} - \text{EMIM}^+ - \text{H}_{\text{C}_2}^+]^{\bullet}$	0		0		0		0	
O-abstraction: $[\text{O} - \text{EMIM}^+ - \text{H}_{\text{C}_2}^+] + \text{NO}$	0		1 ± 1		1 ± 1		0	
HT: $[\text{EMIM}^+ - \text{H}_{\text{C}_2}^+ - \text{H}_{\text{ME}}]^{\bullet} + \text{HONO}$	0		1 ± 1		0		0	
fragmentation of $[\text{EMIM}^+ - \text{H}_{\text{C}_2}^+]$ (elimination of $\text{H}_2$ , $\text{CH}_3$ , and $\text{C}_2\text{H}_5$ )	0		0		3 ± 2		6 ± 2	
							49 ± 5	
								35 ± 5

<sup>a</sup>Percent probabilities and uncertainties were calculated on the basis of 100 trajectories for each condition.

Table 3. Trajectory Reaction Probabilities (%) for MIM + NO<sub>2</sub>, EIM + NO<sub>2</sub> and C<sub>2</sub>H<sub>4</sub> + NO<sub>2</sub> at Various Conditions<sup>a</sup>

temperature (K)	1000	2000	3000	4000	TS <sup>b</sup>		products <sup>b</sup>	
<i>E</i> <sub>col</sub> (eV)	0.5	0.5	0.5	0.5	Δ <i>H</i> (eV)	Δ <i>G</i> (eV)	Δ <i>H</i> (eV)	Δ <i>G</i> (eV)
MIM + NO <sub>2</sub>								
[MIM – H <sub>ME</sub> ] <sup>•</sup> + HONO	0	0	1 ± 1	4 ± 2	0.89	1.34	0.72	0.70
[MIM – H <sub>ME</sub> ] <sup>•</sup> + O–NH–O	0	0	0	0	0.95	1.37	1.03	1.02
[MIM – H <sub>ME</sub> ] <sup>•</sup> + H + NO <sub>2</sub>	0	0	0	9 ± 3			3.98	3.63
[MIM – H <sub>2</sub> ] <sup>•</sup> + H <sub>2</sub> + NO <sub>2</sub>	0	1 ± 1	2 ± 1	9 ± 3			3.41	3.07
[MIM – CH <sub>3</sub> ] <sup>•</sup> + CH <sub>3</sub> + NO <sub>2</sub>	0	0	0	5 ± 2	3.08	3.03	3.23	2.69
short-lived [MIM–ONO] <sup>•</sup>	3 ± 2	2 ± 1	4 ± 2	5 ± 2	1.34	1.87	–0.06	0.20
O–MIM + NO	0	0	0	0	2.21	2.65	0.93	0.97
ring fragmentation	0	0	1 ± 1	7 ± 3				
EIM + NO <sub>2</sub>								
[EIM – H <sup>β</sup> ] <sup>•</sup> + HONO	0	0	0	1 ± 1	1.42	1.80	1.07	1.01
[EIM – H <sup>β</sup> ] <sup>•</sup> + O–NH–O	0	0	0	0	1.30	1.68	1.37	1.33
[EIM – H <sup>β</sup> ] <sup>•</sup> + H + NO <sub>2</sub>	0	0	1 ± 1	3 ± 2			4.32	3.94
[EIM – CH <sub>3</sub> ] <sup>•</sup> + CH <sub>3</sub> + NO <sub>2</sub>	0	0	1 ± 1	2 ± 1			3.32	2.77
[EIM – CH <sub>4</sub> ] <sup>•</sup> + CH <sub>4</sub> + NO <sub>2</sub>	0	0	0	1 ± 1	3.47	3.44	2.82	2.33
[EIM – C <sub>2</sub> H <sub>5</sub> ] <sup>•</sup> + C <sub>2</sub> H <sub>5</sub> + NO <sub>2</sub>	1 ± 1	0	0	7 ± 3			3.17	2.57
2-ethyl-1,3-imidazole	0	0	0	3 ± 2	2.41	2.44	0.56	0.58
ring fragmentation	0	0	1 ± 1	6 ± 2				
C <sub>2</sub> H <sub>4</sub> + NO <sub>2</sub>								
short-lived [CH <sub>2</sub> CH <sub>2</sub> NO <sub>2</sub> ] <sup>•</sup>	1 ± 1	2 ± 1	1 ± 1	1 ± 1				
short-lived [CH <sub>2</sub> CH <sub>2</sub> ONO] <sup>•</sup>	13 ± 2	5 ± 2	5 ± 2	6 ± 2				
[CH <sub>2</sub> CH <sub>2</sub> NO <sub>2</sub> ] <sup>•</sup>	0	0	1 ± 1	1 ± 1	0.51	0.94	0.31	0.81
[CH <sub>2</sub> CH <sub>2</sub> ONO] <sup>•</sup>	0	0	1 ± 1	2 ± 1	1.29	1.50	0.44	0.84

<sup>a</sup>Percent probabilities and uncertainties were calculated on the basis of 100 trajectories for each condition. <sup>b</sup>Structures of all calculated species are available in the Supporting Information.

and EIM + NO<sub>2</sub> at various temperatures and *E*<sub>col</sub> specified in Table 3. Few reactions were observed in these trajectories, most of which are due to the elimination of H, H<sub>2</sub>, methyl, methane, or ethyl from imidazole and ring fragmentation. These reactions have high-lying activation barriers (>3 eV) and endothermicities and therefore are less likely to contribute to the overall reactivity. Short-lived [MIM–ONO]<sup>•</sup> complexes (with ONO bonded to the C2 position) were observed, but none of these converted to a covalent complex or produced O–MIM + NO. EIM may isomerize to 2-ethyl-1,3-imidazole at higher temperatures, but the reaction activation barrier is 2.41 eV.

Among the trajectory-predicted reaction pathways of MIM, the one that may likely contribute to the IL reactivity is methyl-H transfer to form [MIM – H<sub>ME</sub>]<sup>•</sup> + HONO. Interestingly, no nitril hydride (O–NH–O) formation was observed in the HT trajectories, presumably because the formation of O–NH–O requires more energy than that of HONO. A similar HT reaction was observed for EIM, i.e., EIM + NO<sub>2</sub> → [EIM – H<sup>β</sup>]<sup>•</sup> + HONO, although it appears to be disfavored both energetically (with higher activation barrier and endothermicity) and kinetically (only 1% at 4000 K) compared to that for MIM + NO<sub>2</sub>.

**3.4. Reactions of NO<sub>2</sub> with HDCA, Alkyl-DCA, and DCA<sup>–</sup>.** Previously, we had reported dynamics simulations of NO<sub>2</sub> with HDCA and DCA<sup>–</sup> in the 1000–6000 K regime.<sup>10</sup> HDCA + NO<sub>2</sub> has two most important reaction pathways, leading to [HNC(–ONO)NCN]<sup>•</sup> and HNCNC(–ONO)N<sup>•</sup>, respectively. Formation of [HNC(–ONO)NCN]<sup>•</sup> accounted for 3% of the trajectories at 3000 K and *E*<sub>col</sub> = 1.5 eV, and 8% at 6000 K and *E*<sub>col</sub> = 1.5 eV. A large fraction of [HNC(–ONO)NCN]<sup>•</sup> subsequently eliminated NO. Formation of [HNCNC(–ONO)N]<sup>•</sup> was less common and accounted for at most 1% of the trajectories at higher temperatures. The remaining reactive

trajectories could be characterized as HT from HDCA to NO<sub>2</sub> and forming HONO (trajectory probability was 4% at 4000 K, increasing to 11% at 6000 K) or O–NH–O (as a minor process, with a probability of 1–2% at 4000–6000 K). The reaction coordinates and energetics for HDCA + NO<sub>2</sub> are shown in Figure S1 in the Supporting Information. Besides the trajectory-predicted pathways, Figure S1 includes reaction pathways that are initiated at other collision orientations. One surprising finding of comparing the dynamics trajectories with a statistical reaction model is that the trajectory-predicted reactions do not represent minimum energy pathways, and the two lower-energy pathways, leading to the formation of [HNC(–NO<sub>2</sub>)NCN]<sup>•</sup> and [HNCNC(–NO<sub>2</sub>)N]<sup>•</sup>, were not observed in the trajectories. On the basis of the RRKM evaluation of the properties and unimolecular kinetics of nitro (–NO<sub>2</sub>) and nitrite (–ONO) complexes, it was assumed that the shutdown of nitro-complex formation in the trajectories is mainly due to their rapid decomposition (because of the shallow product potential well after the TS that leads to that product). In addition, short-time, nonstatistical collisions of HDCA with NO<sub>2</sub> may result in insufficient intramolecular vibrational redistribution to achieve a statistical situation.

CH<sub>3</sub>DCA and C<sub>2</sub>H<sub>5</sub>DCA are the two products produced from the S<sub>N</sub>2 alkyl abstraction in EMIM<sup>+</sup>DCA<sup>–</sup>. It is reasonable to assume that the two alkyl groups behave similarly in the reaction with NO<sub>2</sub>. Figure 4 shows the reaction profile for CH<sub>3</sub>DCA + NO<sub>2</sub> calculated at the B3LYP/6-311++G(d,p) level of theory. These reactions are similar to those of HDCA + NO<sub>2</sub>, except that the barriers leading to CH<sub>3</sub>NO<sub>2</sub> (via F4.TS6 in Figure 4) and CH<sub>3</sub>ONO (via F4.TS6') become much higher than those in the case of HDCA + NO<sub>2</sub> → O–NH–O + DCA (via FS1.T6 in Figure S1) and HONO + DCA (via FS1.TS6' in Figure S1). Table 4 compares the NO<sub>2</sub> reaction energetics with CH<sub>3</sub>DCA,

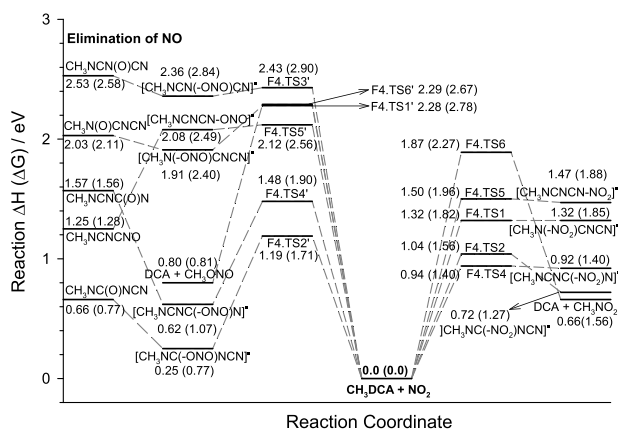


**Figure 4.** Reaction coordinates for  $\text{CH}_3\text{DCA}$  with  $\text{NO}_2$ . Reaction  $\Delta H$  (eV) and  $\Delta G$  (eV, in parentheses) were calculated at the B3LYP/6-311++G(d,p) level of theory, including thermal corrections at 298 K. Cartesian coordinates of stable structures and TSs are provided in the Supporting Information.

$\text{CH}_2=\text{CHCH}_2\text{DCA}$ , and HDCA. The energetically favorable pathways for  $\text{CH}_3\text{DCA}$  correspond to the formation of  $[\text{CH}_3\text{NC}(-\text{ONO})\text{NCN}]^*$ ,  $[\text{CH}_3\text{NCNC}(-\text{ONO})\text{N}]^*$ , and  $[\text{CH}_3\text{NCNC}(-\text{NO}_2)\text{N}]^*$ . However, on the basis of the dominant formation of nitrite complexes over nitro complexes (as a result of nonstatistical kinetics) in the trajectory

simulations of  $\text{HDCA} + \text{NO}_2$  and  $\text{C}_2\text{H}_4 + \text{NO}_2$  (vide infra), we tend to assign  $[\text{CH}_3\text{NC}(-\text{ONO})\text{NCN}]^*$  and  $[\text{CH}_3\text{NCNC}(-\text{ONO})\text{N}]^*$  as the two most probable products of  $\text{CH}_3\text{DCA} + \text{NO}_2$ . Based on the same argument, the most probable product for the reaction of  $\text{C}_2\text{H}_5\text{DCA} + \text{NO}_2$  is  $[\text{C}_2\text{H}_5\text{NC}(-\text{ONO})\text{NCN}]^*$  followed by  $[\text{C}_2\text{H}_5\text{NCNC}(-\text{ONO})\text{N}]^*$ .

The reactivity of  $\text{DCA}^-$  toward  $\text{NO}_2$  is much weaker compared to that of its neutral counterpart HDCA. Few reactions were observed in the collision trajectories of  $\text{DCA}^-$  with  $\text{NO}_2$ , most of which resulted in the formation of short-lived  $[\text{NCNCN}-\text{NO}_2]^{*-}$  and  $[\text{NCNC}(-\text{ONO})\text{N}]^{*-}$ , with probabilities of up to 3%. The reaction coordinates for the trajectory-predicted pathways and the other likely routes are shown in Figure S2 in the Supporting Information. The resulting reaction potential energy diagram shows the repulsive nature for the complex structure of  $[\text{NCNCN}-\text{NO}_2]^{*-}$  (i.e., after taking into account the ZPE and the thermal correction at 298 K, the reaction  $\Delta H$  and  $\Delta G$  values for  $[\text{NCNCN}-\text{NO}_2]^{*-}$  formation are located above the  $\text{NO}_2$ -addition barriers). This suggests that the alternative complex structure  $[\text{NCNC}(-\text{ONO})\text{N}]^{*-}$  (and its dissociation products  $\text{NCNC}(\text{O})\text{N}^- + \text{NO}$ ) may be the most likely outcome of  $\text{DCA}^- + \text{NO}_2$ .

**3.5.  $\text{C}_2\text{H}_4 + \text{NO}_2$ .** This reaction system is relevant to the autoignition and combustion characteristics of fuels in propulsion systems.<sup>49–52</sup> Deng et al.<sup>52</sup> conducted exhaustive calculations for all of the possible reaction pathways between  $\text{C}_2\text{H}_4$  and  $\text{NO}_2$  at the CCSD(T)/CBS//M06-2x/6-311+

**Table 4.** Energies (Units: eV) of TSs and Products for the Reactions of  $\text{NO}_2$  with RDCA vs HDCA<sup>a</sup>

structures	RDCA + $\text{NO}_2$				HDCA + $\text{NO}_2$		
	R = $\text{CH}_3$		R = $\text{CH}_2\text{CHCH}_2$		structures	$\Delta H$	$\Delta G$
F4.TS1	1.32	1.82	1.44	1.91	FS1.TS1	1.33	1.79
$[\text{RN}(-\text{NO}_2)\text{CNCN}]^*$	1.32	1.85	1.29	1.77	$[\text{HN}(-\text{NO}_2)\text{CNCN}]^*$	1.34	1.81
F4.TS2	1.04	1.56	0.98	1.47	FS1.TS2	0.92	1.42
$[\text{RNC}(-\text{NO}_2)\text{NCN}]^*$	0.72	1.27	0.65	1.14	$[\text{HNC}(-\text{NO}_2)\text{NCN}]^*$	0.73	1.24
F4.TS4	0.94	1.40	0.88	1.32	FS1.TS4	0.95	1.44
$[\text{RNCNC}(-\text{NO}_2)\text{N}]^*$	0.92	1.40	0.86	1.31	$[\text{HNCNC}(-\text{NO}_2)\text{N}]^*$	0.93	1.42
F4.TS5	1.50	1.96	1.42	1.82	FS1.TS5	1.50	1.95
$[\text{RNCNCN}-\text{NO}_2]^*$	1.47	1.88	1.39	1.77	$[\text{HNCNCN}-\text{NO}_2]^*$	1.49	1.92
F4.TS6	1.87	2.27	1.60	1.92	FS1.TS6	0.81	1.21
$\text{DCA} + \text{ONO}_2$	0.66	1.56	0.58	0.54	$\text{DCA} + \text{O}-\text{NH}-\text{O}$	0.96	0.95
F4.TS1'	2.28	2.78	2.23	2.68	FS1.TS1'	2.42	2.88
$[\text{RN}(-\text{ONO})\text{CNCN}]^*$	1.91	2.40	1.84	2.29	$[\text{HN}(-\text{ONO})\text{CNCN}]^*$	2.04	2.48
F4.TS2'	1.19	1.71	1.11	1.59	FS1.TS2'	1.23	1.72
$[\text{RNC}(-\text{ONO})\text{NCN}]^*$	0.25	0.77	0.19	0.65	$[\text{HNC}(-\text{ONO})\text{NCN}]^*$	0.32	0.78
F4.TS3'	2.43	2.90	2.37	2.79	FS1.TS3'	2.47	2.92
$[\text{RNCN}(-\text{ONO})\text{CN}]^*$	2.36	2.84	2.30	2.72	$[\text{HNCN}(-\text{ONO})\text{CN}]^*$	2.38	2.83
F4.TS4'	1.48	1.90	1.42	1.79	FS1.TS4'	1.54	1.95
$[\text{RNCNC}(-\text{ONO})\text{N}]^*$	0.62	1.07	0.55	0.95	$[\text{HNCNC}(-\text{ONO})\text{N}]^*$	0.60	1.03
F4.TS5'	2.12	2.56	2.04	2.43	FS1.TS5'	2.11	2.55
$[\text{RNCNCNONO}]^*$	2.08	2.49	2.00	2.38	$[\text{HNCNCNONO}]^*$	2.06	2.48
F4.TS6'	2.29	2.67	1.93	2.27	FS1.TS6'	0.76	1.14
$\text{DCA} + \text{RONO}$	0.80	0.81	0.68	0.63	$\text{DCA} + \text{HONO}$	0.66	0.63
$\text{RN}(\text{O})\text{CNCN} + \text{NO}$	2.03	2.11	1.96	1.98	$\text{HN}(\text{O})\text{CNCN} + \text{NO}$	2.35	2.37
$\text{RNC}(\text{O})\text{NCN} + \text{NO}$	0.66	0.77	0.60	0.65	$\text{HNC}(\text{O})\text{NCN} + \text{NO}$	0.83	0.89
$\text{RNCN}(\text{O})\text{CN} + \text{NO}$	2.53	2.58	2.47	2.45	$\text{HNCN}(\text{O})\text{CN} + \text{NO}$	2.65	2.67
$\text{RNCNC}(\text{O})\text{N} + \text{NO}$	1.57	1.56	1.50	1.45	$\text{HNCNC}(\text{O})\text{N} + \text{NO}$	1.60	1.60
$\text{RNCNCNO} + \text{NO}$	1.25	1.28	1.17	1.15	$\text{HNCNCNO} + \text{NO}$	1.23	1.24

<sup>a</sup>Calculated at the B3LYP/6-311++G(d,p) level of theory, including thermal corrections at 298 K. Structures of all calculated species are available in the Supporting Information.



+G(d,p) levels of theory, wherein the relatively less endothermic pathways (with activation barriers <1.5 eV) involved the formation of  $[\text{C}_2\text{H}_4\text{NO}_2]^*$  and  $[\text{C}_2\text{H}_4\text{ONO}]^*$ , followed by the formation of  $\text{C}_2\text{H}_3 + \text{HONO}$  and  $\text{C}_2\text{H}_3 + \text{O}-\text{NH}-\text{O}$  via HT. We have recalculated the reaction energies for these four pathways at the B3LYP/6-311++G(d,p) level of theory and the results are summarized in Figure 5. The  $[\text{C}_2\text{H}_4\text{ONO}]^*$  may eliminate NO or HNO, and thereby convert to  $\text{CH}_3\text{CHO}$ , epoxide, or  $[\text{CH}_2\text{CHO}]^*$ .

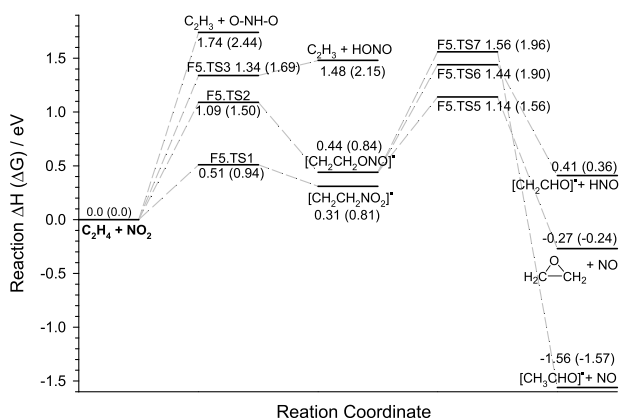
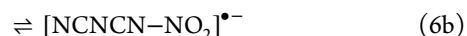
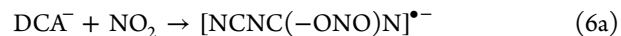
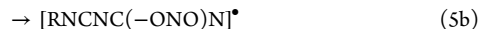
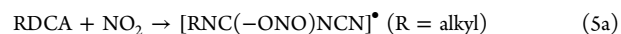
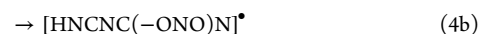
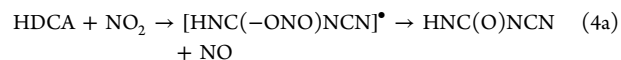
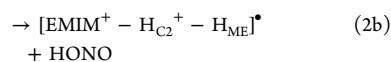
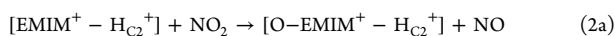
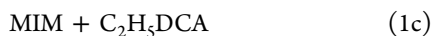
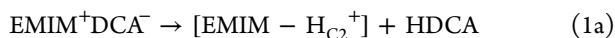


**Figure 5.** Reaction coordinates for  $\text{C}_2\text{H}_4$  with  $\text{NO}_2$ . Reaction  $\Delta H$  (eV) and  $\Delta G$  (eV, in parentheses) were calculated at the B3LYP/6-311++G(d,p) level of theory, including thermal corrections at 298 K. Cartesian coordinates of stable structures and TSs are provided in the Supporting Information.

We have also simulated the collisions of  $\text{C}_2\text{H}_4$  with  $\text{NO}_2$  at temperatures from 1000 to 5000 K and  $E_{\text{col}}$  of 0.5 eV (see Table 3). The most probable reactions corresponded to the formation of  $[\text{CH}_2\text{CH}_2\text{ONO}]^*$  rather than  $[\text{CH}_2\text{CH}_2\text{NO}_2]^*$ , despite the fact that  $[\text{CH}_2\text{CH}_2\text{NO}_2]^*$  is more stable and has half the activation energy compared to  $[\text{CH}_2\text{CH}_2\text{ONO}]^*$ . The non-statistical trajectory outcome of  $\text{C}_2\text{H}_4 + \text{NO}_2$  bears a resemblance to that of  $\text{HDCA} + \text{NO}_2$ . Most of the  $[\text{CH}_2\text{CH}_2\text{ONO}]^*$  formed in the trajectories were short-lived and decayed back to reactants before the end of trajectories; only 2% of the trajectories were able to maintain a stable  $[\text{CH}_2\text{CH}_2\text{ONO}]^*$  structure throughout the trajectory time at 3000 K.

In sum, the synergistic dynamics simulations and reaction coordinate/energetics calculations have predicted the following probable primary and secondary reaction pathways for  $\text{EMIM}^+\text{DCA}^-$  with  $\text{NO}_2$



#### 4. EXTRAPOLATION OF THE $\text{EMIM}^+\text{DCA}^-$ RESULTS TO $\text{BMIM}^+\text{DCA}^-$ AND $\text{AMIM}^+\text{DCA}^-$

**4.1.  $\text{BMIM}^+\text{DCA}^- + \text{NO}_2$ .** It is reasonable to assume that the chemistry of  $\text{BMIM}^+\text{DCA}^-$  with  $\text{NO}_2$  is similar to that of  $\text{EMIM}^+\text{DCA}^-$  with  $\text{NO}_2$ ; consequently, reactions 1–7 of  $\text{EMIM}^+\text{DCA}^- + \text{NO}_2$  were used as the starting points to construct the reaction coordinates for  $\text{BMIM}^+\text{DCA}^- + \text{NO}_2$ . Figure 6 shows the intra-ion-pair reaction coordinates for

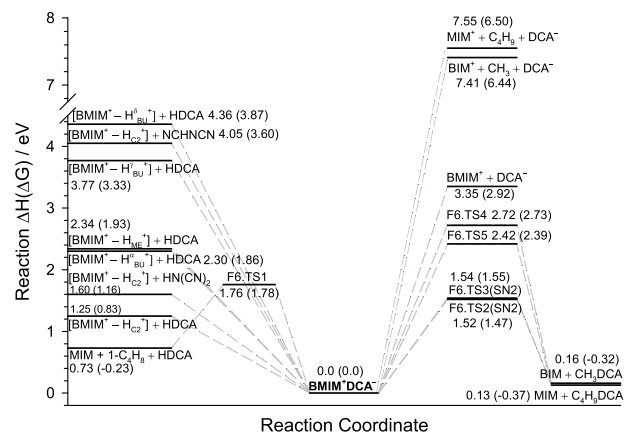


**Figure 6.** Reaction coordinates for the decomposition of  $\text{BMIM}^+\text{DCA}^-$ . Reaction  $\Delta H$  (eV) and  $\Delta G$  (eV, in parentheses) were calculated at the B3LYP/6-311++G(d,p) level of theory, including thermal corrections at 298 K. Cartesian coordinates of stable structures and TSs are provided in the Supporting Information.

$\text{BMIM}^+\text{DCA}^-$ , and the reaction energetics is compiled in Table 5. Reaction  $\Delta H$  and  $\Delta G$  between the same reaction pathways of  $\text{BMIM}^+\text{DCA}^-$  and  $\text{EMIM}^+\text{DCA}^-$  differ only by 0.01–0.1 eV. The favorable pathways of  $\text{BMIM}^+\text{DCA}^-$  are intra-ion-pair PT and alkyl abstraction. PT leads to the formation of  $[\text{BMIM}^+ - \text{H}_{\text{C}_2}^+] + \text{HDCA}$  and  $\text{MIM} + 1\text{-butene} + \text{HDCA}$ . Note in the latter case, the transfer of a butyl- $\text{H}^\beta$  in  $\text{BMIM}^+$  induces the elimination of a 1-butene molecule. Alkyl abstraction in  $\text{BMIM}^+\text{DCA}^-$  is also favored via an  $\text{S}_{\text{N}}2$  mechanism, producing  $\text{MIM} + \text{C}_4\text{H}_9\text{DCA}$  and  $\text{BIM} + \text{CH}_3\text{DCA}$ .

The  $\text{BMIM}^+$ -specific primary products include  $[\text{BMIM}^+ - \text{H}_{\text{C}_2}^+]$ , 1-butene, and BIM. The fact that the trajectory-predicted reactivity of EIM is lower than that of MIM led us to assume that BIM too should be less reactive than MIM and thus was not considered further. Figure 3 compares the reactions of  $\text{NO}_2$  with

Table 5. Comparison of TS and Product Energies (Units: eV) for the Probable Reactions of NO<sub>2</sub> with EMIM<sup>+</sup>DCA<sup>-</sup>, BMIM<sup>+</sup>DCA<sup>-</sup>, and AMIM<sup>+</sup>DCA<sup>-</sup>

pathways	TS ΔH (ΔG)	product ΔH (ΔG)	pathways	TS ΔH (ΔG)	product ΔH (ΔG)	pathways	TS ΔH (ΔG)	product ΔH (ΔG)
EMIM <sup>+</sup> DCA <sup>-</sup> + NO <sub>2</sub>								
[EMIM <sup>+</sup> - H <sub>C2</sub> <sup>+</sup> ] + HDCA	1.68 (1.72)	1.22 (0.81)	[BMIM <sup>+</sup> - H <sub>C2</sub> <sup>+</sup> ] + HDCA	1.76 (1.78)	1.25 (0.83)	[AMIM <sup>+</sup> - H <sub>C2</sub> <sup>+</sup> ] + HDCA	2.09 (2.08)	1.20 (0.77)
MIM + C <sub>2</sub> H <sub>4</sub> + HDCA	1.56 (1.51)	0.85 (-0.08)	MIM + 1-C <sub>4</sub> H <sub>8</sub> + HDCA	1.54 (1.55)	0.73 (-0.23)	MIM + C <sub>3</sub> H <sub>4</sub> + HDCA	1.42 (1.43)	1.01 (0.08)
MIM + C <sub>2</sub> H <sub>3</sub> DCA	1.51 (1.45)	0.11 (-0.37)	MIM + C <sub>4</sub> H <sub>9</sub> DCA	1.52 (1.47)	0.13 (-0.37)	MIM + CH <sub>3</sub> CCH <sub>2</sub> DCA	1.51 (1.46)	0.14 (-0.35)
EIM + CH <sub>3</sub> DCA	[EMIM <sup>+</sup> - H <sub>C2</sub> <sup>+</sup> ] + NO <sub>2</sub>	0.14 (-0.33)	BIM + CH <sub>3</sub> DCA	[BMIM <sup>+</sup> - H <sub>C2</sub> <sup>+</sup> ] + NO <sub>2</sub>	0.16 (-0.32)	AIM + CH <sub>3</sub> DCA	[AMIM <sup>+</sup> - H <sub>C2</sub> <sup>+</sup> ] + NO <sub>2</sub>	0.13 (-0.34)
[O-EMIM <sup>+</sup> - H <sub>C2</sub> <sup>+</sup> ] + NO	0.16 (0.66)	-2.91 (-2.79)	[O-BMIM <sup>+</sup> - H <sub>C2</sub> <sup>+</sup> ] + NO	0.15 (0.62)	-2.82 (-2.80)	[O-AMIM <sup>+</sup> - H <sub>C2</sub> <sup>+</sup> ] + NO	0.18 (0.66)	-2.81 (-2.79)
[EMIM <sup>+</sup> - H <sub>C2</sub> <sup>+</sup> - H <sub>ME</sub> ] <sup>+</sup> + HONO	1.10 (1.53)	0.76 (0.73)	[BMIM <sup>+</sup> - H <sub>C2</sub> <sup>+</sup> - H <sub>ME</sub> ] <sup>+</sup> + HONO	1.10 (1.52)	0.76 (0.73)	[AMIM <sup>+</sup> - H <sub>C2</sub> <sup>+</sup> - H <sub>ME</sub> ] <sup>+</sup> + HONO	1.11 (1.54)	0.76 (0.74)
MIM + NO <sub>2</sub>								
[MIM - H <sub>ME</sub> ] <sup>+</sup> + HONO	0.89 (1.34)	0.72 (0.70)	same	same	same	same	same	same
HDCA + NO <sub>2</sub>								
[HNC(-ONO)NCN] <sup>•</sup>	1.23 (1.72)	0.32 (0.78)	same	same	same	same	same	same
HNC(O)NCN + NO	1.54 (1.95)	0.83 (0.89)	same	same	same	same	same	same
[HNCNC(-ONO)N] <sup>•</sup>	0.76 (1.14)	0.60 (1.03)	same	same	same	same	same	same
DCA + HONO (major)	0.81 (1.21)	0.66 (0.63)	same	same	same	same	same	same
DCA + O-NH-O (minor)	0.81 (1.21)	0.96 (0.95)	same	same	same	same	same	same
C <sub>2</sub> H <sub>3</sub> DCA + NO <sub>2</sub>								
[C <sub>2</sub> H <sub>3</sub> NC(-ONO)NCN] <sup>•</sup>	1.20 (1.72)	0.29 (0.79)	[C <sub>4</sub> H <sub>9</sub> NC(-ONO)NCN] <sup>•</sup>	1.20 (1.72)	0.29 (0.80)	[CH <sub>2</sub> CHCH <sub>2</sub> NC(ONO)NCN] <sup>•</sup>	1.11 (1.57)	0.19 (0.65)
[C <sub>2</sub> H <sub>3</sub> NCNC(-ONO)N] <sup>•</sup>	1.48 (1.90)	0.63 (1.07)	[C <sub>4</sub> H <sub>9</sub> NCNC(-ONO)N] <sup>•</sup>	1.48 (1.89)	0.64 (1.05)	[CH <sub>2</sub> CHCH <sub>2</sub> NCNC(-ONO)N] <sup>•</sup>	1.42 (1.79)	0.55 (0.95)
CH <sub>3</sub> DCA + NO <sub>2</sub>								
[CH <sub>3</sub> NC(-ONO)NCN] <sup>•</sup>	1.19 (1.71)	0.25 (0.77)	same	same	same	same	same	same
[CH <sub>3</sub> NCNC(-ONO)N] <sup>•</sup>	1.48 (1.90)	0.62 (1.07)	same	same	same	same	same	same
C <sub>2</sub> H <sub>4</sub> + NO <sub>2</sub>								
[C <sub>2</sub> H <sub>4</sub> ONO] <sup>•</sup>	1.09 (1.50)	0.44 (0.84)	[C <sub>2</sub> H <sub>5</sub> CH=CH <sub>2</sub> + NO <sub>2</sub>	0.97 (1.39)	0.40 (0.81)	[CH <sub>2</sub> =C=CH <sub>2</sub> + NO <sub>2</sub>	0.68 (1.13)	-0.46 (0.00)
DCA <sup>-</sup> + NO <sub>2</sub>								
[NCNC(-ONO)N] <sup>-</sup>	0.94 (1.38)	0.66 (1.12)	[C <sub>2</sub> H <sub>5</sub> CH(-ONO)CH <sub>3</sub> ] <sup>•</sup>	1.03 (1.47)	0.45 (0.85)	[CH <sub>2</sub> C(-ONO)CH <sub>3</sub> ] <sup>•</sup>		
NCNC(O)N <sup>-</sup> + NO	1.01 (1.44)	1.35 (1.38)	same	same	same	same	same	same
[NCNCN-NO <sub>2</sub> ] <sup>-</sup>	1.01 (1.44)	1.03 (1.45)	same	same	same	same	same	same

[EMIM<sup>+</sup> - H<sub>C2</sub><sup>+</sup>], [BMIM<sup>+</sup> - H<sub>C2</sub><sup>+</sup>], and [AMIM<sup>+</sup> - H<sub>C2</sub><sup>+</sup>], which in the case of [BMIM<sup>+</sup> - H<sub>C2</sub><sup>+</sup>] leads to the formation of [O-BMIM<sup>+</sup> - H<sub>C2</sub><sup>+</sup>] + NO, [O<sub>2</sub>N-BMIM<sup>+</sup> - H<sub>C2</sub><sup>+</sup>]<sup>\*</sup>, and [BMIM<sup>+</sup> - H<sub>C2</sub><sup>+</sup> - H<sub>ME</sub>]<sup>\*</sup> + HONO. The energy differences between the three reaction systems are no more than 0.09 eV. A major difference between BMIM<sup>+</sup>DCA<sup>-</sup> and EMIM<sup>+</sup>DCA<sup>-</sup> concerns the formation of an asymmetrical alkene C<sub>2</sub>H<sub>5</sub>CH=CH<sub>2</sub> in BMIM<sup>+</sup>DCA<sup>-</sup>. NO<sub>2</sub> may attack and attach to either of the two vinyl C atoms in C<sub>2</sub>H<sub>5</sub>CH=CH<sub>2</sub>, and their reaction profiles are illustrated in the two separated frames of Figure 7.

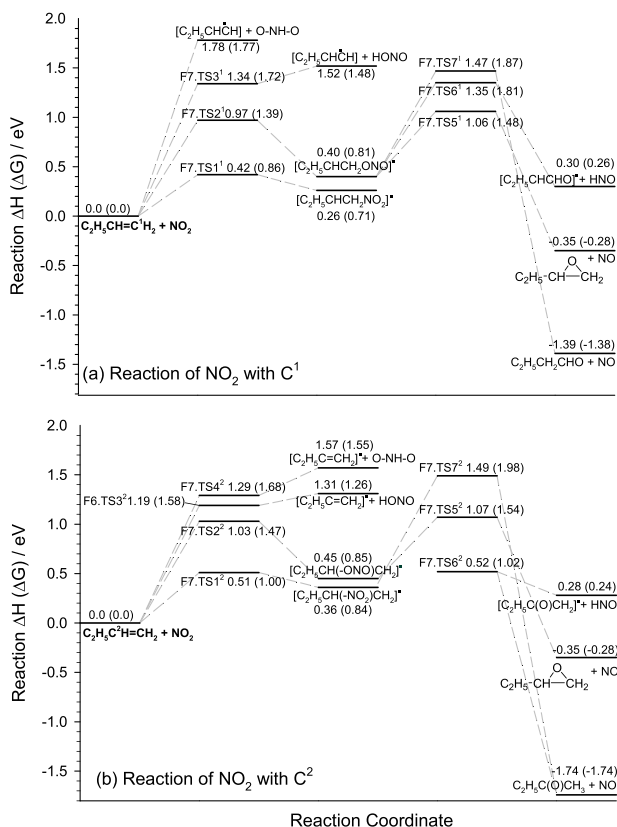


**Figure 7.** Reaction coordinates for 1-butene with NO<sub>2</sub>. Reaction  $\Delta H$  (eV) and  $\Delta G$  (eV, in parentheses) were calculated at the B3LYP/6-311++G(d,p) level of theory, including thermal corrections at 298 K. Cartesian coordinates of stable structures and TSs are provided in the Supporting Information.

For ease of comparison, the TSs for the similar pathways are labeled using the same sequential numbering but differentiated by superscripts, e.g., TS1<sup>1</sup> that leads to [C<sub>2</sub>H<sub>5</sub>CHC<sup>1</sup>H<sub>2</sub>(-NO<sub>2</sub>)]<sup>\*</sup> vs TS1<sup>2</sup> that leads to [C<sub>2</sub>H<sub>5</sub>C<sup>2</sup>H(-NO<sub>2</sub>)C<sup>1</sup>H<sub>2</sub>]<sup>\*</sup>. Both vinyl C may form nitrite and nitro complexes, but C1 appears to be slightly more reactive than C2 as judged by their reaction barriers. The nitro compounds, if formed, may be unstable and quickly decay back to reactants (due to their shallow potential wells with respect to the TSs). As a result, the most probable reactions of 1-butene are 1-C<sub>4</sub>H<sub>8</sub> + NO<sub>2</sub> ⇌ [C<sub>2</sub>H<sub>5</sub>CHCH<sub>2</sub>ONO]<sup>\*</sup> and/or [C<sub>2</sub>H<sub>5</sub>CH(-ONO)-CH<sub>2</sub>]<sup>\*</sup>. BMIM<sup>+</sup>DCA<sup>-</sup> also generates MIM, HDCA, RDCA (R = alkyl), DCA<sup>-</sup>, and alkene. Therefore, reactions 3–7 would be expected in the BMIM<sup>+</sup>DCA<sup>-</sup> system.

**4.2. AMIM<sup>+</sup>DCA<sup>-</sup> + NO<sub>2</sub>.** Guided by the results of the EMIM<sup>+</sup>DCA<sup>-</sup> and BMIM<sup>+</sup>DCA<sup>-</sup> systems, the reaction coordinates for AMIM<sup>+</sup>DCA<sup>-</sup> were constructed at the B3LYP/6-311++G(d,p) level of theory, as shown in Figure 8.

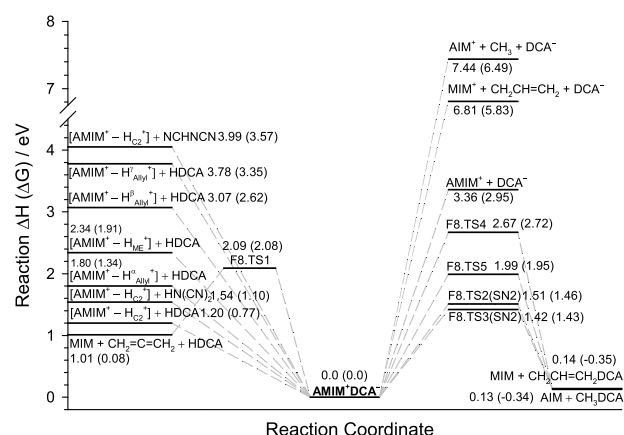


**Figure 8.** Reaction coordinates for the decomposition of AMIM<sup>+</sup>DCA<sup>-</sup>. Reaction  $\Delta H$  (eV) and  $\Delta G$  (eV, in parentheses) were calculated at the B3LYP/6-311++G(d,p) level of theory, including thermal corrections at 298 K. Cartesian coordinates of stable structures and TSs are provided in the Supporting Information.

AMIM<sup>+</sup>DCA<sup>-</sup> indeed is seen to similarly follow the most probable pathways as those of EMIM<sup>+</sup>DCA<sup>-</sup> and BMIM<sup>+</sup>DCA<sup>-</sup>, including intra-ion-pair PT that leads to [AMIM - H<sub>C2</sub><sup>+</sup>] + HDCA and MIM + allene + HDCA and S<sub>N</sub>2 alkyl abstraction that leads to MIM + CH<sub>2</sub>CHCH<sub>2</sub>DCA and AIM + CH<sub>3</sub>DCA. We have compared in Table 5 the reaction pathways and products for all of the three dialkylimidazolium–DCA ILs.

AMIM<sup>+</sup>-specific PT products are [AMIM - H<sub>C2</sub><sup>+</sup>] and allene. The common reaction pathways for NO<sub>2</sub> with [EMIM - H<sub>C2</sub><sup>+</sup>], [BMIM - H<sub>C2</sub><sup>+</sup>], and [AMIM - H<sub>C2</sub><sup>+</sup>] are illustrated in Figure 3. Figure 9 focuses on the NO<sub>2</sub> reactions with the allyl in [AMIM - H<sub>C2</sub><sup>+</sup>], and Figure 10 on the NO<sub>2</sub> reactions with allene. NO<sub>2</sub> may attack the allyl C<sup>β</sup> and C<sup>γ</sup> atoms, forming nitrite and nitro complexes followed by NO elimination. Considering the reaction energetics and the nonstatistical kinetics of NO<sub>2</sub> addition, the most likely NO<sub>2</sub>-adducts to the allyl of [AMIM - H<sub>C2</sub><sup>+</sup>] are [(MIM<sup>+</sup> - H<sub>C2</sub><sup>+</sup>)CH<sub>2</sub>CHCH<sub>2</sub>ONO]<sup>\*</sup> and [(MIM<sup>+</sup> - H<sub>C2</sub><sup>+</sup>)CH<sub>2</sub>CH(-ONO)CH<sub>2</sub>]<sup>\*</sup>. We also examined the reactivity of the allyl group in AMIM<sup>+</sup> and compared this to that in [AMIM - H<sub>C2</sub><sup>+</sup>] in Table 6. The two allyl groups present the same reaction routes with NO<sub>2</sub>, but the allyl in AMIM<sup>+</sup> appears to be less reactive than that in [AMIM<sup>+</sup> - H<sub>C2</sub><sup>+</sup>] as inferred from its relatively high TSs and product  $\Delta H$ s (0.1–0.2 eV higher than those for [AMIM<sup>+</sup> - H<sub>C2</sub><sup>+</sup>]).

## 5. COMPARISON WITH EXPERIMENTS

**5.1. Reactivities of BMIM<sup>+</sup>DCA<sup>-</sup>, AMIM<sup>+</sup>DCA<sup>-</sup>, and MAT<sup>+</sup>DCA<sup>-</sup>.** Kaiser et al.'s experiments on the NO<sub>2</sub> oxidation of MAT<sup>+</sup>DCA<sup>-</sup>,<sup>9</sup> BMIM<sup>+</sup>DCA<sup>-</sup>,<sup>11</sup> and AMIM<sup>+</sup>DCA<sup>-</sup><sup>12</sup> revealed the following facts: (1) DCA<sup>-</sup> reacts with NO<sub>2</sub> to a greater extent than the cations. (2) The reactions involved the bonding of the nitrogen dioxide N and/or O to an imidazolium C or N. The infrared and Raman spectra of the oxidation products suggested the formation of nitrites (RONO), nitroamines (RR'NNO<sub>2</sub>), aromatic nitro compounds (ArNO<sub>2</sub>), and carbonitrates (RR'C=NO<sub>2</sub><sup>-</sup>), as well as a carbonyl group in higher-order products. (3) By measuring the decrease of reactant Raman intensities at 2192 (sym CN stretch of DCA<sup>-</sup>) and 1011 cm<sup>-1</sup> ( $\delta$  ring mode of BMIM<sup>+</sup>) and the increase of the product Raman intensities at 1698, 1603, and 1219 cm<sup>-1</sup>, the reaction rate constant of BMIM<sup>+</sup>DCA<sup>-</sup> was determined to be (1.5–2.5) × 10<sup>-3</sup> s<sup>-1</sup>. The measurement was

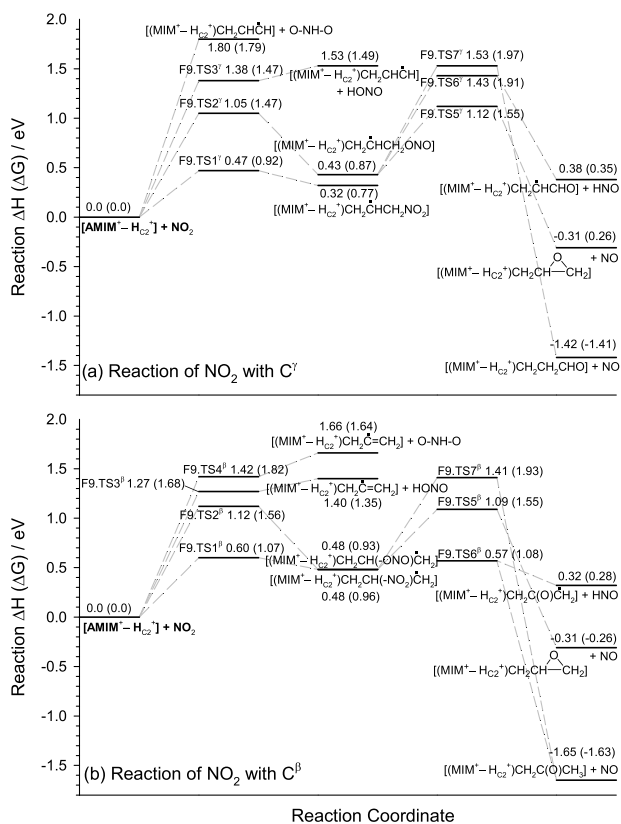


**Figure 9.** Reaction coordinates for  $\text{NO}_2$  with the allyl group of  $[\text{AMIM}^+ - \text{H}_{\text{C}_2}^+]$ . Reaction  $\Delta H$  (eV) and  $\Delta G$  (eV, in parentheses) were calculated at the B3LYP/6-311++G(d,p) level of theory, including thermal corrections at 298 K. Cartesian coordinates of stable structures and TSs are provided in the Supporting Information.

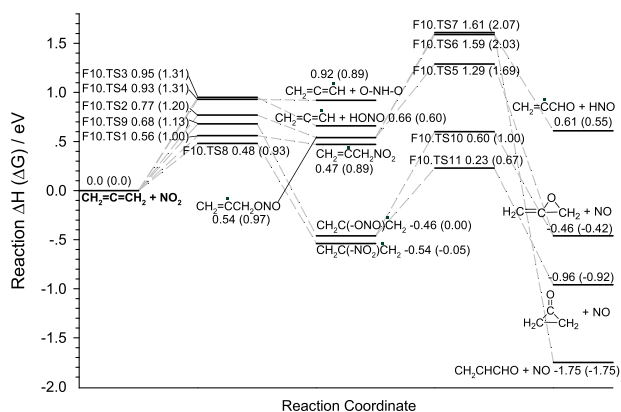


**Figure 10.** Reaction coordinates for allene with  $\text{NO}_2$ . Reaction  $\Delta H$  (eV) and  $\Delta G$  (eV, in parentheses) were calculated at the B3LYP/6-311++G(d,p) level of theory, including thermal corrections at 298 K. Cartesian coordinates of stable structures and TSs are provided in the Supporting Information.

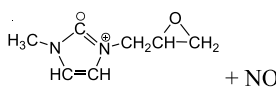
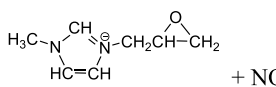
made at 298 K with a  $\text{NO}_2$  concentration of 0.2%. For comparison, the rate constant of  $\text{MAT}^+\text{DCA}^-$  was measured to be  $(7.3\text{--}10.4) \times 10^{-5} \text{ s}^{-1}$  under the same experimental conditions,<sup>9</sup> and so the rate constant is a factor of  $\sim 20$  lower for  $\text{MAT}^+\text{DCA}^-$  than that for  $\text{BMIM}^+\text{DCA}^-$ . The rate constant of  $\text{AMIM}^+\text{DCA}^-$  was measured at 308 K with a  $\text{NO}_2$  concentration of 0.4%. After correcting for the different temperatures and  $\text{NO}_2$  concentrations, the actual rate constant for  $\text{AMIM}^+\text{DCA}^-$  is lower than that for  $\text{BMIM}^+\text{DCA}^-$  by a

factor of 2. Thus, the order of reactivity with  $\text{NO}_2$  decreases in the order of  $\text{BMIM}^+\text{DCA}^- > \text{AMIM}^+\text{DCA}^- \gg \text{MAT}^+\text{DCA}^-$ .

The reactions of  $\text{BMIM}^+\text{DCA}^-$ ,  $\text{AMIM}^+\text{DCA}^-$ , and  $\text{MAT}^+\text{DCA}^-$  are all initiated by intra-ion-pair PT (and alkyl abstraction for  $\text{BMIM}^+\text{DCA}^-$  and  $\text{AMIM}^+\text{DCA}^-$ ), leading to the formation of HDCA, alkyl-DCA,  $[1,3\text{-dialkylimidazolium}^+ - \text{H}_{\text{C}_2}^+]$ ,  $[\text{MAT}^+ - \text{H}_{\text{C}_5}^+]$ , etc., followed by the reactions of the primary products with  $\text{NO}_2$ . The different reactivities among the three ILs originate from their different cation structures.  $\text{BMIM}^+$  and  $\text{AMIM}^+$  differ from  $\text{MAT}^+$  in that the amino group of  $\text{MAT}^+$  is, respectively, replaced by a butyl and an allyl group and that the imidazolium ring has one less N atom than the triazolium ring. Consequently, each IL presents some unique reaction pathways and intermediates as follows: (1)  $\text{BMIM}^+$  has a total of 13 H (methyl-H, butyl-H, and  $\text{H}_{\text{C}_2}$ ) available for PT followed by 9 in  $\text{AMIM}^+$  (methyl-H, allyl-H, and  $\text{H}_{\text{C}_2}$ ) and then 6 in  $\text{MAT}^+$  ( $\text{C}_5\text{-H}$ , amino-H, and methyl-H). Moreover, a unique intra-ion-pair PT in  $\text{BMIM}^+\text{DCA}^-$  and  $\text{AMIM}^+\text{DCA}^-$  is the concerted  $\text{H}^\beta$ -transfer and elimination of  $1\text{-C}_4\text{H}_8$  or  $\text{CH}_2=\text{C}=\text{CH}_2$ . To this end,  $\text{BMIM}^+$  has two butyl- $\text{H}^\beta$  available for PT, whereas  $\text{AMIM}^+$  has only one allyl- $\text{H}^\beta$  available for PT (i.e., the reaction statistical factor of  $\text{H}^\beta$ -PT is 2 for  $\text{BMIM}^+$  and 1 for  $\text{AMIM}^+$ ), and the reaction is exoergic for  $\text{BMIM}^+\text{DCA}^-$  but slightly endoergic for  $\text{AMIM}^+\text{DCA}^-$ . Consequently,  $\text{BMIM}^+\text{DCA}^-$  is more reactive than  $\text{AMIM}^+\text{DCA}^-$ . (2) In contrast to  $\text{MAT}^+\text{DCA}^-$ , both  $\text{BMIM}^+\text{DCA}^-$  and  $\text{AMIM}^+\text{DCA}^-$  have exoergic  $\text{S}_{\text{N}}2$  alkyl abstraction reactions, which release heat that can promote other reactions and thus account for their higher reactivities than  $\text{MAT}^+\text{DCA}^-$ . (3) The ion binding energies of  $\text{BMIM}^+\text{DCA}^-$  and  $\text{AMIM}^+\text{DCA}^-$  are  $\Delta H = 3.35\text{--}3.36$  eV and  $\Delta G = 2.92\text{--}2.95$  eV, and those of  $\text{MAT}^+\text{DCA}^-$  are  $\Delta H = 3.97$  eV and  $\Delta G = 3.49$  eV, respectively,<sup>10</sup> which makes the  $\text{DCA}^-$  in  $\text{MAT}^+\text{DCA}^-$  more strongly paired with the cation and less accessible to the reaction with  $\text{NO}_2$ . (4) Following the TS theory-based rate constant  $k(T) = \frac{k_{\text{B}}T}{h} e^{-(\Delta G^\ddagger(T)/k_{\text{B}}T)}$  ( $k_{\text{B}}$  is Boltzmann's constant,  $h$  is Planck's constant, and  $T$  is the temperature),<sup>53</sup> the measured rate constants of  $\text{BMIM}^+\text{DCA}^-$  and  $\text{AMIM}^+\text{DCA}^-$  correspond to overall barriers of 0.92 and 0.94 eV, respectively. As there are multiple primary and higher-order reactions in the ILs, these activation barriers cannot be simply related to a particular reaction, but the measured barriers are comparable to the primary reactions of  $\text{BMIM}^+\text{DCA}^-$  and  $\text{AMIM}^+\text{DCA}^-$  listed in Table 5.

**5.2. Product Infrared and Raman Spectra.** To compare with Kaiser et al.'s spectroscopic measurements of the  $\text{BMIM}^+\text{DCA}^-$  and  $\text{AMIM}^+\text{DCA}^-$  droplets reacting with  $\text{NO}_2$ , we calculated vibrational frequencies and their infrared absorptivities and Raman scattering activities for  $\text{BMIM}^+\text{DCA}^-$ ,  $\text{AMIM}^+\text{DCA}^-$ , and their reaction products using the SMD-GIL//M06/6-311++G(d,p) method. The surrounding IL solvation shell was defined as  $\epsilon$  (static dielectric constant of the solvent) = 11.5,  $n^2$  (dynamic dielectric constant) = 2.0449,  $\alpha$  (H bond acidity) = 0.229,  $\beta$  (H bond basicity) = 0.265,  $\gamma$  (surface tension at interface) = 61.24,  $\varphi$  (carbon aromaticity) = 0.2308, and  $\psi$  (electronegative halogenicity) = 0.0000.<sup>46</sup> In a previous work,<sup>10</sup> we calculated both harmonic and anharmonic vibrations of  $\text{MAT}^+\text{DCA}^-$ . It turned out that the harmonic infrared and Raman data better matched the spectra of the levitated IL droplet. Therefore, only the harmonic spectra were chosen for the spectral analysis in the present work. The calculated vibrational frequencies were scaled by an empirical

Table 6. Energies (Units: eV) of TSs and Products for the Reactions of NO<sub>2</sub> with [AMIM<sup>+</sup> - H<sub>C2</sub><sup>+</sup>] vs AMIM<sup>+</sup> <sup>a</sup>

[AMIM <sup>+</sup> - H <sub>C2</sub> <sup>+</sup> ] + NO <sub>2</sub>			AMIM <sup>+</sup> + NO <sub>2</sub>		
Structures	ΔH	ΔG	Structures	ΔH	ΔG
[(MIM <sup>+</sup> - H <sub>C2</sub> <sup>+</sup> )CH <sub>2</sub> CHCH] <sup>+</sup> + O-NH-O	1.80	1.79	[MIM <sup>+</sup> CH <sub>2</sub> CHCH] <sup>+</sup> + O-NH-O	1.87	1.86
F9.TS1 <sup>γ</sup>	0.47	0.92	TS1 <sup>γ</sup>	0.64	1.11
[(MIM <sup>+</sup> - H <sub>C2</sub> <sup>+</sup> )CH <sub>2</sub> CHCH <sub>2</sub> NO <sub>2</sub> ] <sup>+</sup>	0.32	0.77	[MIM <sup>+</sup> CH <sub>2</sub> CHCH <sub>2</sub> NO <sub>2</sub> ] <sup>+</sup>	0.50	0.94
F9.TS2 <sup>γ</sup>	1.05	1.47	TS2 <sup>γ</sup>	1.35	1.77
[(MIM <sup>+</sup> - H <sub>C2</sub> <sup>+</sup> )CH <sub>2</sub> CHCH <sub>2</sub> ONO] <sup>+</sup>	0.43	0.87	[MIM <sup>+</sup> CH <sub>2</sub> CHCH <sub>2</sub> ONO] <sup>+</sup>	0.54	0.96
F9.TS3 <sup>γ</sup>	1.38	1.47	TS3 <sup>γ</sup>	1.62	2.01
[(MIM <sup>+</sup> - H <sub>C2</sub> <sup>+</sup> )CH <sub>2</sub> CHCH] <sup>+</sup> + HONO	1.53	1.49	[MIM <sup>+</sup> CH <sub>2</sub> CHCH] <sup>+</sup> + HONO	1.61	1.57
F9.TS5 <sup>γ</sup>	1.12	1.55	TS5 <sup>γ</sup>	1.12	1.55
 + NO	-0.31	0.26	 + NO	-0.16	-0.10
F9.TS6 <sup>γ</sup>	1.43	1.91	TS6 <sup>γ</sup>	1.65	2.12
[(MIM <sup>+</sup> - H <sub>C2</sub> <sup>+</sup> )CH <sub>2</sub> CHCHO] <sup>+</sup> + HNO	0.38	0.35	[MIM <sup>+</sup> CH <sub>2</sub> CHCHO] <sup>+</sup> + HNO	0.72	0.18
F9.TS7 <sup>γ</sup>	1.53	1.97	TS7 <sup>γ</sup>	1.82	2.19
[(MIM <sup>+</sup> - H <sub>C2</sub> <sup>+</sup> )CH <sub>2</sub> CH <sub>2</sub> CHO] + NO	-1.42	-1.41	MIM <sup>+</sup> CH <sub>2</sub> CH <sub>2</sub> CHO + NO	-1.29	-1.27
F9.TS1 <sup>β</sup>	0.60	1.07	TS1 <sup>β</sup>	0.82	1.31
[(MIM <sup>+</sup> - H <sub>C2</sub> <sup>+</sup> )CH <sub>2</sub> CH(-NO <sub>2</sub> )CH <sub>2</sub> ] <sup>+</sup>	0.48	0.96	[MIM <sup>+</sup> CH <sub>2</sub> CH(-NO <sub>2</sub> )CH <sub>2</sub> ] <sup>+</sup>	0.59	1.10
F9.TS2 <sup>β</sup>	1.12	1.56	TS2 <sup>β</sup>	1.38	1.81
[(MIM <sup>+</sup> - H <sub>C2</sub> <sup>+</sup> )CH <sub>2</sub> CH(-ONO)CH <sub>2</sub> ] <sup>+</sup>	0.48	0.93	[MIM <sup>+</sup> CH <sub>2</sub> CH(-ONO)CH <sub>2</sub> ] <sup>+</sup>	0.67	1.11
F9.TS3 <sup>β</sup>	1.27	1.68	TS3 <sup>β</sup>	1.45	1.82
[(MIM <sup>+</sup> - H <sub>C2</sub> <sup>+</sup> )CH <sub>2</sub> C=CH <sub>2</sub> ] <sup>+</sup> + HONO	1.40	1.35	[MIM <sup>+</sup> CH <sub>2</sub> C=CH <sub>2</sub> ] <sup>+</sup> + HONO	1.46	1.41
F9.TS4 <sup>β</sup>	1.42	1.82	TS4 <sup>β</sup>	1.59	2.01
[(MIM <sup>+</sup> - H <sub>C2</sub> <sup>+</sup> )CH <sub>2</sub> C=CH <sub>2</sub> ] <sup>+</sup> + O-NH-O	1.66	1.64	[MIM <sup>+</sup> CH <sub>2</sub> C=CH <sub>2</sub> ] <sup>+</sup> + O-NH-O	1.73	1.70
F9.TS5 <sup>β</sup>	1.09	1.55	TS5 <sup>β</sup>	1.13	1.57
F9.TS6 <sup>β</sup>	0.57	1.08	TS6 <sup>β</sup>	0.71	1.20
[(MIM <sup>+</sup> - H <sub>C2</sub> <sup>+</sup> )CH <sub>2</sub> C(O)CH <sub>2</sub> ] <sup>+</sup> + HNO	0.32	0.28	MIM <sup>+</sup> CH <sub>2</sub> C(O)CH <sub>2</sub> + HNO	0.63	0.59
F9.TS7 <sup>β</sup>	1.41	1.93	TS7 <sup>β</sup>	1.69	2.17
[(MIM <sup>+</sup> - H <sub>C2</sub> <sup>+</sup> )CH <sub>2</sub> C(O)CH <sub>3</sub> ] + NO	-1.65	-1.63	MIM <sup>+</sup> CH <sub>2</sub> C(O)CH <sub>3</sub> + NO	-1.65	-1.63

<sup>a</sup>Calculated at the B3LYP/6-311++G(d,p) level of theory, including thermal corrections at 298 K. Structures of all calculated species are available in the Supporting Information.

factor of 0.957, which was determined by least-squares fitting of the calculated BMIM<sup>+</sup>DCA<sup>-</sup> and AMIM<sup>+</sup>DCA<sup>-</sup> vibrations to the experimental values. Accuracies of the theoretically predicted frequencies were evaluated using root-mean-square (RMSD) =  $\sqrt{\frac{1}{m} \sum_{i=1}^m (\nu_{i,\text{cal}} - \nu_{i,\text{expt}})^2}$ , where  $m$  is the total number of vibrations for comparison, and  $\nu_{i,\text{cal}}$  and  $\nu_{i,\text{expt}}$  are the scaled SMD-GIL/M06/6-311++G(d,p) and experimental frequencies, respectively. RMSD is 25 cm<sup>-1</sup> for infrared and 23 cm<sup>-1</sup> for Raman. The harmonic bands of BMIM<sup>+</sup>DCA<sup>-</sup> and AMIM<sup>+</sup>DCA<sup>-</sup> were then convoluted using Gaussian curves with a full width at half-maximum (FWHM) of 32 cm<sup>-1</sup> to best match the experimental linewidths. The resulting infrared and Raman spectra are compared with the experimental spectra in Figures S3 and S4 in the Supporting Information. The assignments in Tables S1–S4 are based on the experimental data. Note that, while vibrational frequencies can be predicted with fairly high accuracy, vibrational intensities often cannot be.

Figure 11 presents the simulated infrared (in the top frame of each figure) and Raman (in the bottom frame) spectra for the primary and secondary products of BMIM<sup>+</sup>DCA<sup>-</sup> and AMIM<sup>+</sup>DCA<sup>-</sup>, each of which corresponds to a specific type of reaction as we have described for EMIM<sup>+</sup>DCA<sup>-</sup> and is labeled accordingly. Peaks that are close to or overlap with experimental BMIM<sup>+</sup>DCA<sup>-</sup> (or AMIM<sup>+</sup>DCA<sup>-</sup>) vibrations and consequently were obscured by the reactant peaks in the measurements are labeled in black. Peaks that match the new product peaks detected in the experiment (within the stated RMSD) are labeled in red. As we will present below, each of the new experimental IR and Raman peaks can be attributed to one or more reaction products and to N<sub>2</sub>O<sub>4</sub> (which is in equilibrium with NO<sub>2</sub>). Note that infrared and Raman follow different selection rules and some vibrations have nearly identical frequencies; as a result, a calculated frequency may correspond to a black-labeled peak in the infrared spectrum and a red-labeled peak in Raman spectrum (and vice versa). Occasionally,

BMIM<sup>+</sup>DCA<sup>-</sup> products

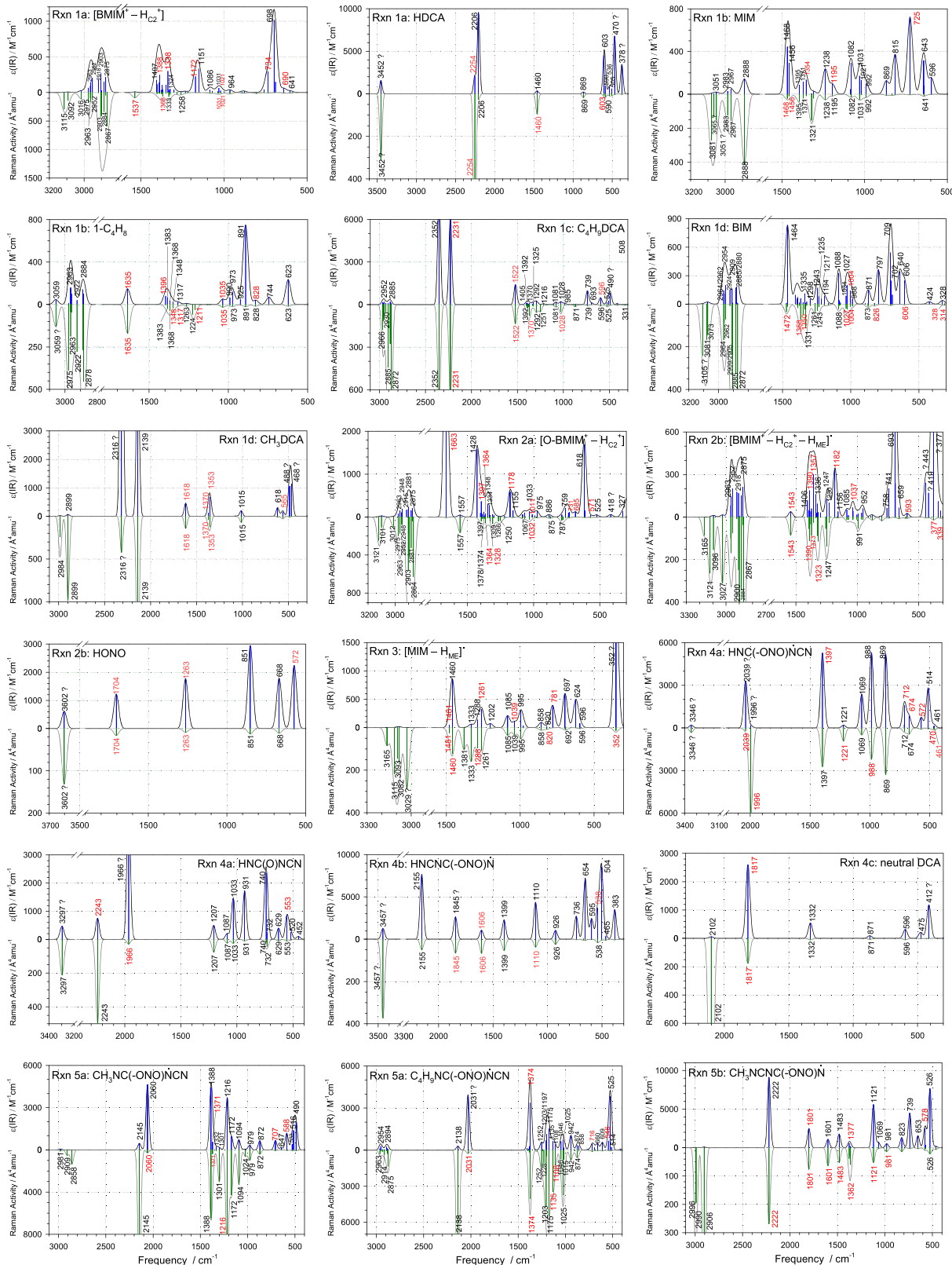


Figure 11. continued

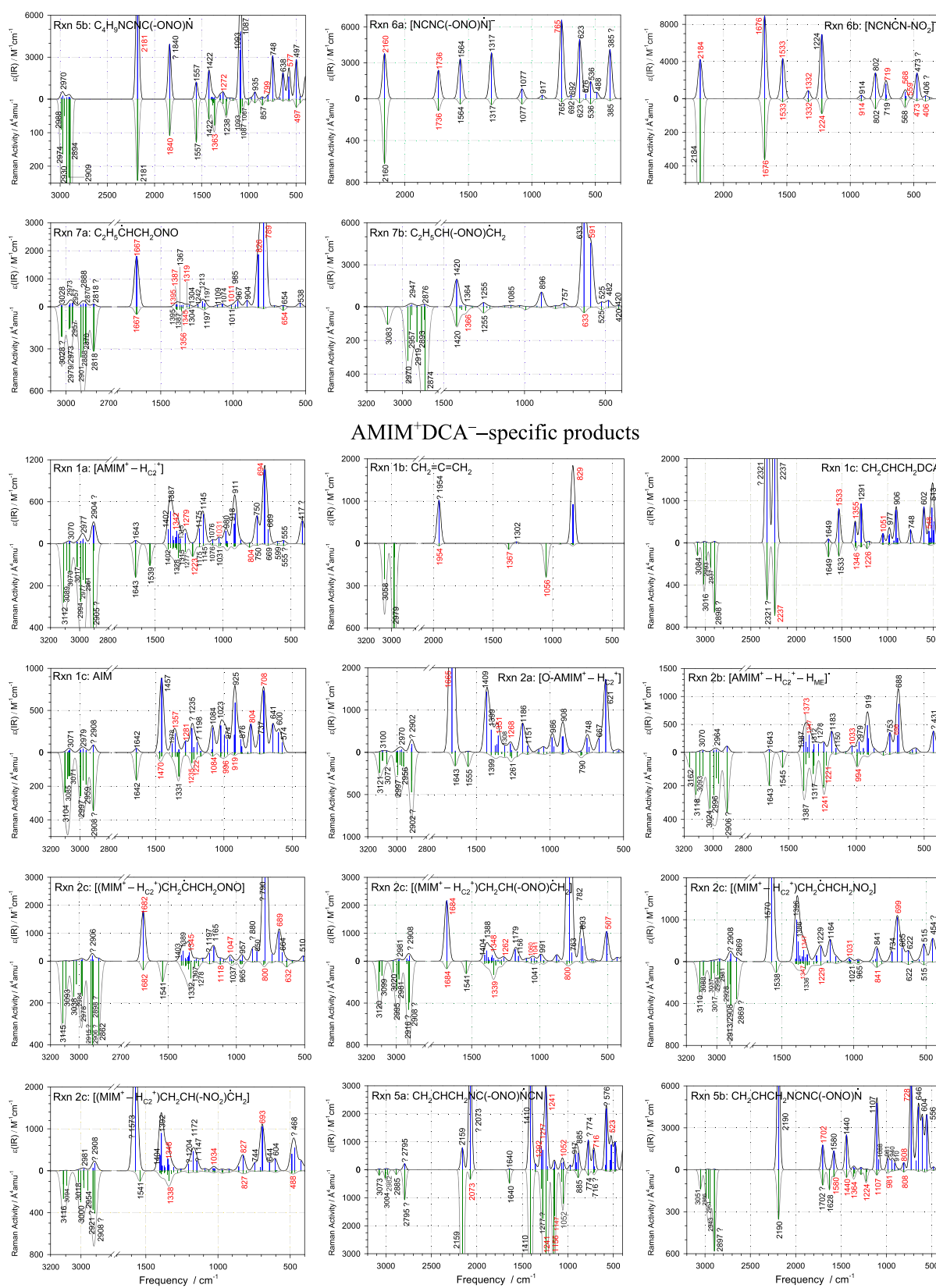
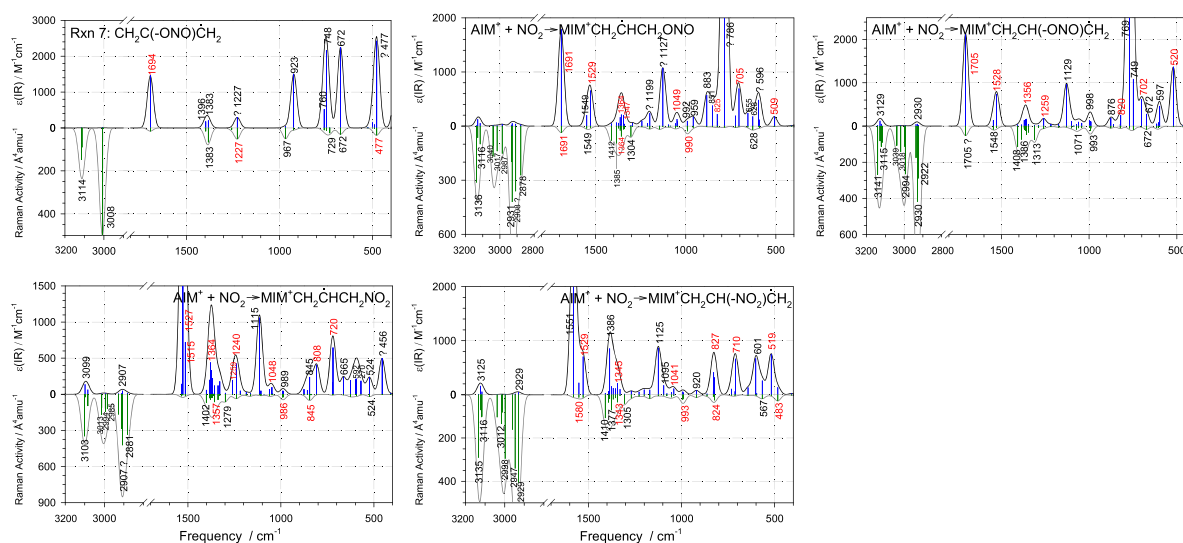


Figure 11. continued



**Figure 11.** SMD-GIL//M06/6-311++G(d,p)-simulated infrared (top) and Raman (bottom) spectra of theoretically predicted products, where the Franck–Condon gaps are omitted. Frequencies were scaled by a factor of 0.957. Red-labeled peaks match experimental products and black-labeled ones are close to reactant IL vibrations. Peaks that do not match experimental data are indicated with question marks.

there are peaks that do not match any of the experimentally detected vibrations and thus are labeled with question marks. The origin of mismatches could be due to the combined uncertainties of experiments and theory.

**5.2.1. Product Spectra for  $\text{BMIM}^+\text{DCA}^- + \text{NO}_2$ .** Assignments of specific products were made by matching the simulated product spectral features with the experimental measurements (see Table 7). The product pair of  $[\text{BMIM}^+ - \text{H}_{\text{C}_2}^+] + \text{HDCA}$ , produced from the intra-ion-pair PT (similar to those in reaction 1a of  $\text{EMIM}^+\text{DCA}^-$ ), have numerous vibrational peaks that were identified in the experiment. This indicates that they are among the most probable products detected in the experiment. Their characteristic IR peaks include 1388 (strong, ring swinging), 1338 (strong,  $\text{CH}_2$  wagging), 1172 (strong,  $\text{CH}_2$  twisting), 1021 (ring H–CC–H scissoring,  $\text{CH}_3$  rocking, and CN stretch), 734 (ring torsion), and  $690 \text{ cm}^{-1}$  ( $\text{CH}_2$  rocking) for  $[\text{BMIM}^+ - \text{H}_{\text{C}_2}^+]$  and  $2254 \text{ cm}^{-1}$  (asym N–C–N stretch) for HDCA. Their distinguishable Raman peaks include 1537 (ring CC stretch), 1368 ( $\text{CH}_2$  scissoring), 1031 (ring H–CC–H scissoring), and  $1021 \text{ cm}^{-1}$  for  $[\text{BMIM}^+ - \text{H}_{\text{C}_2}^+]$  and 2254 (strong), 1460 (asym C–N–C stretch), and  $603 \text{ cm}^{-1}$  (C–N–H bending) for HDCA. Besides, HDCA has NH stretch ( $3452 \text{ cm}^{-1}$ ), swing ( $470 \text{ cm}^{-1}$ ), and rocking ( $378 \text{ cm}^{-1}$ ), which were all beyond the experimental detection range.

The product pair of  $\text{MIM} + 1\text{-C}_4\text{H}_8$ , similar to those in reaction 1b, also present vibrations that match the experimental results. These include IR peaks at 1354 ( $\text{CH}_3$  umbrella), 1195 (ring CH rocking), and  $725 \text{ cm}^{-1}$  (strong, ring CH out-of-plane wagging) for MIM and at 1635 (strong, CC stretch), 1396 ( $\text{CH}_2$  scissoring), 1035 (CC stretch and  $\text{CH}_3$  rocking), and  $828 \text{ cm}^{-1}$  ( $\text{CH}_3$  and  $\text{CH}_2$  rocking) for  $1\text{-C}_4\text{H}_8$ , and Raman peaks at 1468 (sym ring C–N–C stretch) and  $1456 \text{ cm}^{-1}$  (asym ring stretch) for MIM and at 1635 (strong), 1348 ( $\text{CH}_2$  scissoring), 1317 ( $\text{CH}_3$  umbrella), 1211 ( $\text{CH}_2$  twisting), and  $1035 \text{ cm}^{-1}$  for  $1\text{-C}_4\text{H}_8$ .

$\text{C}_4\text{H}_9\text{DCA}$  represents a specific product of butyl abstraction (similar to that in reaction 1c). It displays three IR peaks at 2231 (strong, asym N–C–N stretch), 1522 (DCA CN stretch), and  $596 \text{ cm}^{-1}$  (bending of DCA N–C–N) and four Raman peaks at 2231 (strong), 1522, 1370 ( $\text{CH}_2$  scissoring), and  $1028 \text{ cm}^{-1}$

(C–DCA stretch) that match the experimental data, suggesting its detection in the experiment.

BIM and  $\text{CH}_3\text{DCA}$  represent the methyl abstraction products (similar to those in reaction 1d). Identification of BIM in the actual products was based on its IR peak at  $1004 \text{ cm}^{-1}$  (ring CH–N–CH scissoring) and Raman peaks at 1472 (ring CC stretch), 1368 ( $\text{CH}_2$  scissoring), 1350 (asym ring C–N–C stretch), 1027 (ring H–CC–H scissoring), 1004 (sym HC–N–CH stretch), 826 (out-of-plane twisting of ring H–CC–H), 606 (ring out-of-plane distortion), 328 (C–DCA bending), and  $314 \text{ cm}^{-1}$  (butyl bending); and that of  $\text{CH}_3\text{DCA}$  was based on its IR peaks at 1618 (sym N–C–N stretch), 1370 ( $\text{CH}_2$  scissoring), 1353 ( $\text{CH}_3$  bending), and  $563 \text{ cm}^{-1}$  (DCA twisting), and Raman peaks at 1618, 1370, and  $1353 \text{ cm}^{-1}$ .

The products from the  $\text{NO}_2$  reactions with  $[\text{BMIM}^+ - \text{H}_{\text{C}_2}^+]$  (similar to those as in reactions 2a,b) include  $[\text{O-BMIM}^+ - \text{H}_{\text{C}_2}^+]$ ,  $[\text{BMIM}^+ - \text{H}_{\text{C}_2}^+ - \text{H}_{\text{ME}}]^\bullet$ , HONO, and NO. NO may correspond to the  $1907 \text{ cm}^{-1}$  peak<sup>54</sup> in the product Raman spectrum.  $[\text{O-BMIM}^+ - \text{H}_{\text{C}_2}^+]$  has IR peaks at 1663 (strong, CO stretch), 1397 (methyl bending), 1391 ( $\text{CH}_3$  wagging), 1364 ( $\text{CH}_2$  scissoring), 1178 (ring H–CC–H rock), 1011 (ring H–CC–H bending), 731 (ring out-of-plane twisting and  $\text{CH}_2$  rocking), 685 ( $\text{CH}_2$  rock), and  $571 \text{ cm}^{-1}$  (ring out-of-plane twisting) and Raman peaks at 1364, 1328 (ring CN stretch), and  $1032 \text{ cm}^{-1}$  (asym C–C–C stretch) that match the experimental data.  $[\text{BMIM}^+ - \text{H}_{\text{C}_2}^+ - \text{H}_{\text{ME}}]^\bullet$  has product-matching IR peaks at 1543 (ring C=C stretch), 1390 ( $\text{CH}_2$  scissoring), 1357 (strong,  $\text{CH}_2$  scissoring and ring H–CC–H rocking), 1182 (strong, ring H–CC–H rocking), 1037 (ring H–CC–H bending), and  $593 \text{ cm}^{-1}$  (ring out-of-plane twisting) and Raman peaks at 1543, 1390 (strong), 1373 (ring stretch and  $\text{CH}_2$  scissoring), 1323 (strong, CN stretch and  $=\text{CH}_2$  scissoring), 377 ( $\text{CH}_2$  out-of-plane wagging), and  $339 \text{ cm}^{-1}$  ( $\text{CH}_2$  out-of-plane twisting). The IR peaks of HONO at 1704 (O–N stretch), 1263 (strong, OH in-plane rocking), and  $572 \text{ cm}^{-1}$  (strong, OH out-of-plane rocking) and the Raman peaks of HONO at 1704 and  $1263 \text{ cm}^{-1}$  have close matches in the experimental spectra, suggesting that the reaction of the 2b type occurred in the experiment. Note that *cis*-HONO (not shown in Figure 11), which is 0.04 eV higher in energy than the



Table 7. Assignments of the New Vibrational Peaks Detected in the Experiment of BMIM<sup>+</sup>DCA<sup>-</sup> + NO<sub>2</sub>

IR <sup>a</sup> (cm <sup>-1</sup> )	possible attributions <sup>b</sup>	Raman <sup>a</sup> (cm <sup>-1</sup> )	possible attributions <sup>b</sup>
2260	HDCA	2221	HDCA, C <sub>4</sub> H <sub>9</sub> DCA, [CH <sub>3</sub> NCNC(-ONO)N] <sup>+</sup>
2240	C <sub>4</sub> H <sub>9</sub> DCA, HNC(O)NCN	2038	[HNC(-ONO)NCN] <sup>+</sup> , [CH <sub>3</sub> NC(-ONO)NCN] <sup>+</sup> , [C <sub>4</sub> H <sub>9</sub> NC(-ONO)NCN] <sup>+</sup>
2192	HNCNC(O)N, [C <sub>4</sub> H <sub>9</sub> NCNC(-ONO)N] <sup>+</sup> , [NCNCN-NO <sub>2</sub> ] <sup>-</sup>	1981	[HNC(-ONO)NCN] <sup>+</sup>
2170	[C <sub>4</sub> H <sub>9</sub> NCNC(-ONO)N] <sup>+</sup> , [NCNC(-ONO)N] <sup>+</sup>	1947	HNC(O)NCN
1787	DCA, [CH <sub>3</sub> NCNC(-ONO)N] <sup>+</sup> , N <sub>2</sub> O <sub>4</sub>	1907	NO
1745	[NCNC(-ONO)N] <sup>+</sup> , N <sub>2</sub> O <sub>4</sub>	1869	[HNCNC(-ONO)C] <sup>+</sup> , [C <sub>4</sub> H <sub>9</sub> NCNC(-ONO)N] <sup>+</sup>
1714	HONO, N <sub>2</sub> O <sub>4</sub>	1789	DCA, [CH <sub>3</sub> NCNC(-ONO)N] <sup>+</sup>
1652	[O-BMIM <sup>+</sup> - H <sub>CE</sub> ] <sup>+</sup> , <i>cis</i> -HONO, NCNCN-NO <sub>2</sub> <sup>-</sup> , [C <sub>2</sub> H <sub>5</sub> CHCH <sub>2</sub> ONO] <sup>+</sup>	1725	HONO, [NCNC(-ONO)N] <sup>+</sup> , NCNC(O)N <sup>-</sup>
1624	1-C <sub>4</sub> H <sub>9</sub> , CH <sub>3</sub> DCA, [HNCNC(-ONO)N] <sup>+</sup>	1653	1-C <sub>4</sub> H <sub>9</sub> , <i>cis</i> -HONO, [NCNCN-NO <sub>2</sub> ] <sup>-</sup> , [C <sub>2</sub> H <sub>5</sub> CHCH <sub>2</sub> ONO] <sup>+</sup>
1532	C <sub>4</sub> H <sub>9</sub> DCA, [BMIM <sup>+</sup> - H <sub>CE</sub> ] <sup>+</sup> , [MIM - H <sub>ME</sub> ] <sup>+</sup> , [NCNCN-NO <sub>2</sub> ] <sup>-</sup>	1616	CH <sub>3</sub> DCA, [HNCNC(-ONO)N] <sup>+</sup> , [CH <sub>3</sub> NCNC(-ONO)N] <sup>+</sup>
1510	[MIM - H <sub>ME</sub> ] <sup>+</sup>	1584	[CH <sub>3</sub> NCNC(-ONO)N] <sup>+</sup>
1393	[BMIM <sup>+</sup> - H <sub>CE</sub> ] <sup>+</sup> , 1-C <sub>4</sub> H <sub>9</sub> , [O-BMIM <sup>+</sup> - H <sub>CE</sub> ] <sup>+</sup> , [BMIM <sup>+</sup> - H <sub>CE</sub> ] <sup>+</sup> , [HNC(-ONO)NCN] <sup>+</sup> , [C <sub>2</sub> H <sub>5</sub> CHCH <sub>2</sub> ONO] <sup>+</sup>	1535	[BMIM <sup>+</sup> - H <sub>CE</sub> ] <sup>+</sup> , C <sub>4</sub> H <sub>9</sub> DCA, [BMIM <sup>+</sup> - H <sub>CE</sub> ] <sup>+</sup> , [MIM - H <sub>ME</sub> ] <sup>+</sup> , [NCNCN-NO <sub>2</sub> ] <sup>-</sup>
1364	MIM, CH <sub>3</sub> DCA, [O-BMIM <sup>+</sup> - H <sub>CE</sub> ] <sup>+</sup> , [BMIM <sup>+</sup> - H <sub>CE</sub> ] <sup>+</sup> , [MIM - H <sub>ME</sub> ] <sup>+</sup> , [CH <sub>3</sub> NC(-ONO)NCN] <sup>+</sup> , [CH <sub>3</sub> NCNC(-ONO)N] <sup>+</sup> , [C <sub>4</sub> H <sub>9</sub> NC(-ONO)NCN] <sup>+</sup> , [C <sub>2</sub> H <sub>5</sub> CHCH <sub>2</sub> ONO] <sup>+</sup>	1492	[MIM - H <sub>ME</sub> ] <sup>+</sup> , [CH <sub>3</sub> NCNC(-ONO)N] <sup>+</sup>
1323	[BMIM <sup>+</sup> - H <sub>CE</sub> ] <sup>+</sup> , [NCNCN-NO <sub>2</sub> ] <sup>-</sup> , [C <sub>2</sub> H <sub>5</sub> CHCH <sub>2</sub> ONO] <sup>+</sup>	1470	HDCA, MIM, BIM, [MIM - H <sub>ME</sub> ] <sup>+</sup>
1266	HONO, <i>cis</i> -HONO, [MIM - H <sub>ME</sub> ] <sup>+</sup> , C <sub>4</sub> H <sub>9</sub> NCNC(-ONO)N <sup>+</sup>	1436	MIM
1185	[BMIM <sup>+</sup> - H <sub>CE</sub> ] <sup>+</sup> , MIM, [O-BMIM <sup>+</sup> - H <sub>CE</sub> ] <sup>+</sup> , [BMIM <sup>+</sup> - H <sub>CE</sub> ] <sup>+</sup> , [MIM - H <sub>ME</sub> ] <sup>+</sup>	1361	[BMIM <sup>+</sup> - H <sub>CE</sub> ] <sup>+</sup> , 1-C <sub>4</sub> H <sub>9</sub> , C <sub>4</sub> H <sub>9</sub> DCA, BIM, CH <sub>3</sub> DCA, [O-BMIM <sup>+</sup> - H <sub>CE</sub> ] <sup>+</sup> , [BMIM <sup>+</sup> - H <sub>CE</sub> ] <sup>+</sup> , [MIM - H <sub>ME</sub> ] <sup>+</sup> , [CH <sub>3</sub> NC(-ONO)NCN] <sup>+</sup> , [CH <sub>3</sub> NCNC(-ONO)N] <sup>+</sup> , [C <sub>4</sub> H <sub>9</sub> NC(-ONO)NCN] <sup>+</sup> , [C <sub>2</sub> H <sub>5</sub> CHCH <sub>2</sub> ONO] <sup>+</sup>
1041	1-C <sub>4</sub> H <sub>9</sub> , [BMIM <sup>+</sup> - H <sub>CE</sub> ] <sup>+</sup> , [MIM - H <sub>ME</sub> ] <sup>+</sup>	1323	1-C <sub>4</sub> H <sub>9</sub> , [O-BMIM <sup>+</sup> - H <sub>CE</sub> ] <sup>+</sup> , [BMIM <sup>+</sup> - H <sub>CE</sub> ] <sup>+</sup> , [MIM - H <sub>ME</sub> ] <sup>+</sup>
1007	[BMIM <sup>+</sup> - H <sub>CE</sub> ] <sup>+</sup> , BIM, [O-BMIM <sup>+</sup> - H <sub>CE</sub> ] <sup>+</sup> , [C <sub>2</sub> H <sub>5</sub> CHCH <sub>2</sub> ONO] <sup>+</sup>	1284	HONO, <i>cis</i> -HONO, [MIM - H <sub>ME</sub> ] <sup>+</sup>
827	1-C <sub>4</sub> H <sub>9</sub> , [C <sub>2</sub> H <sub>5</sub> CHCH <sub>2</sub> ONO] <sup>+</sup>	1218	1-C <sub>4</sub> H <sub>9</sub> , [HNC(-ONO)NCN] <sup>+</sup> , [CH <sub>3</sub> NC(-ONO)NCN] <sup>+</sup> , [NCNCN-NO <sub>2</sub> ] <sup>-</sup> , [C <sub>2</sub> H <sub>5</sub> CHCH <sub>2</sub> ONO] <sup>+</sup>
790	[MIM - H <sub>ME</sub> ] <sup>+</sup> , [C <sub>4</sub> H <sub>9</sub> NCNC(-ONO)N] <sup>+</sup> , [C <sub>2</sub> H <sub>5</sub> CHCH <sub>2</sub> ONO] <sup>+</sup>	1138	[C <sub>4</sub> H <sub>9</sub> NC(-ONO)NCN] <sup>+</sup>
773	[NCNC(-ONO)N] <sup>+</sup>	1115	HNCNC(-ONO)N <sup>+</sup> , [CH <sub>3</sub> NCNC(-ONO)N] <sup>+</sup> , [C <sub>4</sub> H <sub>9</sub> NC(-ONO)NCN] <sup>+</sup>
740	[BMIM <sup>+</sup> - H <sub>CE</sub> ] <sup>+</sup> , MIM, [O-BMIM <sup>+</sup> - H <sub>CE</sub> ] <sup>+</sup> , [HNC(-ONO)NCN] <sup>+</sup> , [C <sub>4</sub> H <sub>9</sub> NC(-ONO)NCN] <sup>+</sup> , [NCNCN-NO <sub>2</sub> ] <sup>-</sup>	1052	[BMIM <sup>+</sup> - H <sub>CE</sub> ] <sup>+</sup> , 1-C <sub>4</sub> H <sub>8</sub>
680	[BMIM <sup>+</sup> - H <sub>CE</sub> ] <sup>+</sup> , [O-BMIM <sup>+</sup> - H <sub>CE</sub> ] <sup>+</sup> , [HNC(-ONO)NCN] <sup>+</sup> , [CH <sub>3</sub> NC(-ONO)NCN] <sup>+</sup>	1019	[BMIM <sup>+</sup> - H <sub>CE</sub> ] <sup>+</sup> , 1-C <sub>4</sub> H <sub>9</sub> , C <sub>4</sub> H <sub>9</sub> DCA, BIM, [O-BMIM <sup>+</sup> - H <sub>CE</sub> ] <sup>+</sup>
583	C <sub>4</sub> H <sub>9</sub> DCA, [O-BMIM <sup>+</sup> - H <sub>CE</sub> ] <sup>+</sup> , [BMIM <sup>+</sup> - H <sub>CE</sub> ] <sup>+</sup> , [MIM - H <sub>ME</sub> ] <sup>+</sup> , HONO, [HNC(-ONO)NCN] <sup>+</sup> , [CH <sub>3</sub> NC(-ONO)NCN] <sup>+</sup> , [CH <sub>3</sub> NCNC(-ONO)N] <sup>+</sup> , [C <sub>4</sub> H <sub>9</sub> NCNC(-ONO)N] <sup>+</sup> , [NCNCN-NO <sub>2</sub> ] <sup>-</sup> , [C <sub>2</sub> H <sub>5</sub> CH(-ONO)CH <sub>2</sub> ] <sup>+</sup>	964	[HNC(-ONO)NCN] <sup>+</sup> , [CH <sub>3</sub> NCNC(-ONO)N] <sup>+</sup>
555	CH <sub>3</sub> DCA, HNC(O)NCN, [HNCNC(-ONO)N] <sup>+</sup> , HONO, [C <sub>4</sub> H <sub>9</sub> NC(-ONO)NCN] <sup>+</sup> , [NCNCN-NO <sub>2</sub> ] <sup>-</sup>	903	[NCNCN-NO <sub>2</sub> ] <sup>-</sup>
		820	BIM, [MIM - H <sub>ME</sub> ] <sup>+</sup>
		650	[C <sub>2</sub> H <sub>5</sub> CHCH <sub>2</sub> ONO] <sup>+</sup> , [C <sub>2</sub> H <sub>5</sub> CH(-ONO)CH <sub>2</sub> ] <sup>+</sup>
		603	HDCA, BIM
		491	[HNC(-ONO)NCN] <sup>+</sup> , [C <sub>4</sub> H <sub>9</sub> NCNC(-ONO)N] <sup>+</sup>
		465	[HNC(-ONO)NCN] <sup>+</sup> , [NCNCN-NO <sub>2</sub> ] <sup>-</sup>
		410	[NCNCN-NO <sub>2</sub> ] <sup>-</sup>
		350	[BMIM <sup>+</sup> - H <sub>CE</sub> ] <sup>+</sup> , [MIM - H <sub>ME</sub> ] <sup>+</sup>
		328	BIM, [BMIM <sup>+</sup> - H <sub>CE</sub> ] <sup>+</sup> , [MIM - H <sub>ME</sub> ] <sup>+</sup>
		310	BIM

<sup>a</sup>Ref 11. <sup>b</sup>The species in bold has a dominating IR or Raman intensity at the assigned frequency.

Table 8. Assignments of the New Vibrational Peaks Detected in the Experiment of AMIM<sup>+</sup>DCA<sup>-</sup> + NO<sub>2</sub>

IR <sup>a</sup> (cm <sup>-1</sup> )	Possible attributions <sup>b</sup>	Raman <sup>a</sup> (cm <sup>-1</sup> )	Possible attributions <sup>b</sup>
Frequencies that appear in both EMIM <sup>+</sup> DCA <sup>-</sup> + NO <sub>2</sub> and BMIM <sup>+</sup> DCA <sup>-</sup> + NO <sub>2</sub> . The common products thereof are indicated in the gray-shaded cells.			
2260	<b>HDCA</b>	2230	<b>HDCA, [CH<sub>3</sub>NCNC(-ONO)N]<sup>+</sup></b> <b>CH<sub>2</sub>CHCH<sub>2</sub>DCA</b>
1789	<b>DCA, [CH<sub>3</sub>NCNC(-ONO)N]<sup>+</sup>, N<sub>2</sub>O<sub>4</sub></b>	2020	[HNC(-ONO)NCN] <sup>+</sup> , [CH <sub>3</sub> NC(-ONO)NCN] <sup>+</sup> ,
1749	<b>[NCNC(-ONO)N]<sup>+</sup>, N<sub>2</sub>O<sub>4</sub></b>	1867	[HNCNC(-ONO)N] <sup>+</sup>
1716	<b>HONO, N<sub>2</sub>O<sub>4</sub></b>	1662	<i>cis</i> -HONO, <b>[NCNCN-NO<sub>2</sub>]<sup>+</sup></b> [(MIM <sup>+</sup> - H <sub>C2</sub> <sup>+</sup> )CH <sub>2</sub> CHCH <sub>2</sub> ONO] <sup>+</sup> , [(MIM <sup>+</sup> - H <sub>C2</sub> <sup>+</sup> )CH <sub>2</sub> CH(-ONO)CH <sub>2</sub> ] <sup>+</sup> , [MIM <sup>+</sup> CH <sub>2</sub> CHCH <sub>2</sub> ONO] <sup>+</sup>
1524	<b>[NCNCN-NO<sub>2</sub>]<sup>+</sup></b> <b>CH<sub>2</sub>CHCH<sub>2</sub>DCA,</b> [MIM <sup>+</sup> CH <sub>2</sub> CHCH <sub>2</sub> ONO] <sup>+</sup> , <b>[MIM<sup>+</sup>CH<sub>2</sub>CH(-ONO)CH<sub>2</sub>]<sup>+</sup>,</b> <b>[MIM<sup>+</sup>CH<sub>2</sub>CHCH<sub>2</sub>NO<sub>2</sub>]<sup>+</sup>,</b> [MIM <sup>+</sup> CH <sub>2</sub> CH(-NO <sub>2</sub> )CH <sub>2</sub> ] <sup>+</sup>	1352	<b>CH<sub>3</sub>DCA, [CH<sub>3</sub>NC(-ONO)NCN]<sup>+</sup>,</b> <b>[CH<sub>3</sub>NCNC(-ONO)N]<sup>+</sup></b> CH <sub>2</sub> =C=CH <sub>2</sub> , CH <sub>2</sub> CHCH <sub>2</sub> DCA, [MIM <sup>+</sup> - H <sub>C2</sub> <sup>+</sup> ]CH <sub>2</sub> CH(-ONO)CH <sub>2</sub> <sup>+</sup> , [(MIM <sup>+</sup> - H <sub>C2</sub> <sup>+</sup> )CH <sub>2</sub> CHCH <sub>2</sub> NO <sub>2</sub> ] <sup>+</sup> , [(MIM <sup>+</sup> - H <sub>C2</sub> <sup>+</sup> )CH <sub>2</sub> CH(-NO <sub>2</sub> )CH <sub>2</sub> ] <sup>+</sup> , [CH <sub>2</sub> CHCH <sub>2</sub> NCNC(-ONO)N] <sup>+</sup> , [MIM <sup>+</sup> CH <sub>2</sub> CHCH <sub>2</sub> ONO] <sup>+</sup> , [MIM <sup>+</sup> CH <sub>2</sub> CHCH <sub>2</sub> NO <sub>2</sub> ] <sup>+</sup> , [MIM <sup>+</sup> CH <sub>2</sub> CH(-NO <sub>2</sub> )CH <sub>2</sub> ] <sup>+</sup>
1356	MIM, <b>CH<sub>3</sub>DCA,</b> [CH <sub>3</sub> NC(-ONO)NCN] <sup>+</sup> , [CH <sub>3</sub> NCNC(-ONO)N] <sup>+</sup> [AMIM <sup>+</sup> - H <sub>C2</sub> <sup>+</sup> ], <b>CH<sub>2</sub>CHCH<sub>2</sub>DCA,</b> AIM, [O-AMIM <sup>+</sup> - H <sub>C2</sub> <sup>+</sup> ], [AMIM <sup>+</sup> - H <sub>C2</sub> <sup>+</sup> - H <sub>ME</sub> ] <sup>+</sup> , [(MIM <sup>+</sup> - H <sub>C2</sub> <sup>+</sup> )CH <sub>2</sub> CHCH <sub>2</sub> ONO] <sup>+</sup> , [(MIM <sup>+</sup> - H <sub>C2</sub> <sup>+</sup> )CH <sub>2</sub> CH(-ONO)CH <sub>2</sub> ] <sup>+</sup> , [(MIM <sup>+</sup> - H <sub>C2</sub> <sup>+</sup> )CH <sub>2</sub> CHCH <sub>2</sub> NO <sub>2</sub> ] <sup>+</sup> , [(MIM <sup>+</sup> - H <sub>C2</sub> <sup>+</sup> )CH <sub>2</sub> CH(-NO <sub>2</sub> )CH <sub>2</sub> ] <sup>+</sup> , [MIM <sup>+</sup> CH <sub>2</sub> CHCH <sub>2</sub> ONO] <sup>+</sup> , [MIM <sup>+</sup> CH <sub>2</sub> CH(-ONO)CH <sub>2</sub> ] <sup>+</sup> , <b>[MIM<sup>+</sup>CH<sub>2</sub>CHCH<sub>2</sub>NO<sub>2</sub>]<sup>+</sup>,</b> [MIM <sup>+</sup> CH <sub>2</sub> CH(-NO <sub>2</sub> )CH <sub>2</sub> ] <sup>+</sup>	1218	<b>[HNC(-ONO)NCN]<sup>+</sup>, [CH<sub>3</sub>NC(-ONO)NCN]<sup>+</sup>,</b> <b>[NCNCN-NO<sub>2</sub>]<sup>+</sup></b> [AMIM <sup>+</sup> - H <sub>C2</sub> <sup>+</sup> ], CH <sub>2</sub> CHCH <sub>2</sub> DCA, AIM, <b>[AMIM<sup>+</sup> - H<sub>C2</sub><sup>+</sup> - H<sub>ME</sub>]<sup>+</sup>,</b> [(MIM <sup>+</sup> - H <sub>C2</sub> <sup>+</sup> )CH <sub>2</sub> CHCH <sub>2</sub> NO <sub>2</sub> ] <sup>+</sup> , <b>[CH<sub>2</sub>CHCH<sub>2</sub>NC(-ONO)NCN]<sup>+</sup>,</b> [CH <sub>2</sub> CHCH <sub>2</sub> NCNC(-ONO)N] <sup>+</sup> , [CH <sub>2</sub> C(-ONO)CH <sub>2</sub> ] <sup>+</sup>
1269	<b>HONO, <i>cis</i>-HONO, [MIM - H<sub>ME</sub>]<sup>+</sup></b> [AMIM <sup>+</sup> - H <sub>C2</sub> <sup>+</sup> ], AIM, [O-AMIM <sup>+</sup> - H <sub>C2</sub> <sup>+</sup> ], [(MIM <sup>+</sup> - H <sub>C2</sub> <sup>+</sup> )CH <sub>2</sub> CH(-ONO)CH <sub>2</sub> ] <sup>+</sup> , <b>[CH<sub>2</sub>CHCH<sub>2</sub>NC(-ONO)NCN]<sup>+</sup>,</b> <b>[MIM<sup>+</sup>CH<sub>2</sub>CH(-ONO)CH<sub>2</sub>]<sup>+</sup>, [MIM<sup>+</sup>CH<sub>2</sub>CHCH<sub>2</sub>NO<sub>2</sub>]<sup>+</sup></b>	492	[HNC(-ONO)NCN] <sup>+</sup> [(MIM <sup>+</sup> - H <sub>C2</sub> <sup>+</sup> )CH <sub>2</sub> CH(-NO <sub>2</sub> )CH <sub>2</sub> ] <sup>+</sup> , [CH <sub>2</sub> C(-ONO)CH <sub>2</sub> ] <sup>+</sup> , [MIM <sup>+</sup> CH <sub>2</sub> CH(-NO <sub>2</sub> )CH <sub>2</sub> ] <sup>+</sup>
1040	[MIM - H <sub>ME</sub> ] <sup>+</sup> [AMIM <sup>+</sup> - H <sub>C2</sub> <sup>+</sup> ], CH <sub>2</sub> CHCH <sub>2</sub> DCA, [AMIM <sup>+</sup> - H <sub>C2</sub> <sup>+</sup> - H <sub>ME</sub> ] <sup>+</sup> , [(MIM <sup>+</sup> - H <sub>C2</sub> <sup>+</sup> )CH <sub>2</sub> CHCH <sub>2</sub> ONO] <sup>+</sup> , [(MIM <sup>+</sup> - H <sub>C2</sub> <sup>+</sup> )CH <sub>2</sub> CH(-ONO)CH <sub>2</sub> ] <sup>+</sup> , [(MIM <sup>+</sup> - H <sub>C2</sub> <sup>+</sup> )CH <sub>2</sub> CHCH <sub>2</sub> NO <sub>2</sub> ] <sup>+</sup> , [(MIM <sup>+</sup> - H <sub>C2</sub> <sup>+</sup> )CH <sub>2</sub> CH(-NO <sub>2</sub> )CH <sub>2</sub> ] <sup>+</sup> , [CH <sub>2</sub> CHCH <sub>2</sub> NC(-ONO)NCN] <sup>+</sup> , [MIM <sup>+</sup> CH <sub>2</sub> CHCH <sub>2</sub> ONO] <sup>+</sup> , [MIM <sup>+</sup> CH <sub>2</sub> CHCH <sub>2</sub> NO <sub>2</sub> ] <sup>+</sup> , [MIM <sup>+</sup> CH <sub>2</sub> CH(-NO <sub>2</sub> )CH <sub>2</sub> ] <sup>+</sup>	416	[NCNCN-NO <sub>2</sub> ] <sup>+</sup>
AMIM <sup>+</sup> -specific peaks			
1680	<b>[O-AMIM<sup>+</sup> - H<sub>C2</sub><sup>+</sup>], [(MIM<sup>+</sup> - H<sub>C2</sub><sup>+</sup>)CH<sub>2</sub>CHCH<sub>2</sub>ONO]<sup>+</sup>,</b> <b>[(MIM<sup>+</sup> - H<sub>C2</sub><sup>+</sup>)CH<sub>2</sub>CH(-ONO)CH<sub>2</sub>]<sup>+</sup>,</b> <b>[CH<sub>2</sub>CHCH<sub>2</sub>NCNC(-ONO)N]<sup>+</sup>,</b> <b>[CH<sub>2</sub>C(-ONO)CH<sub>2</sub>]<sup>+</sup>,</b> <b>[MIM<sup>+</sup>CH<sub>2</sub>CHCH<sub>2</sub>ONO]<sup>+</sup>,</b> <b>[MIM<sup>+</sup>CH<sub>2</sub>CH(-ONO)CH<sub>2</sub>]<sup>+</sup></b>	2095	[CH <sub>2</sub> CHCH <sub>2</sub> NC(-ONO)NCN] <sup>+</sup>

Table 8. continued

IR <sup>a</sup> (cm <sup>-1</sup> )	Possible attributions <sup>b</sup>	Raman <sup>a</sup> (cm <sup>-1</sup> )	Possible attributions <sup>b</sup>
1613		1964	<b>CH<sub>2</sub>=C=CH<sub>2</sub></b> ,
827	<b>CH<sub>2</sub>=C=CH<sub>2</sub></b> , AIM, [(MIM <sup>+</sup> - H <sub>C2</sub> <sup>+</sup> )CH <sub>2</sub> CH(-NO <sub>2</sub> )CH <sub>2</sub> ] <sup>+</sup> , [CH <sub>2</sub> CHCH <sub>2</sub> NCNC(-ONO)N] <sup>+</sup> , [MIM <sup>+</sup> CH <sub>2</sub> CHCH <sub>2</sub> ONO] <sup>+</sup> , [MIM <sup>+</sup> CH <sub>2</sub> CH(-ONO)CH <sub>2</sub> ] <sup>+</sup> , [MIM <sup>+</sup> CH <sub>2</sub> CHCH <sub>2</sub> NO <sub>2</sub> ] <sup>+</sup> , <b>MIM<sup>+</sup>CH<sub>2</sub>CH(-NO<sub>2</sub>)CH<sub>2</sub></b>	1773	<b>N<sub>2</sub>O<sub>4</sub></b>
711	[AMIM <sup>+</sup> - H <sub>C2</sub> <sup>+</sup> ], AIM, [AMIM <sup>+</sup> - H <sub>C2</sub> <sup>+</sup> - H <sub>ME</sub> ] <sup>+</sup> , [(MIM <sup>+</sup> - H <sub>C2</sub> <sup>+</sup> )CH <sub>2</sub> CHCH <sub>2</sub> ONO] <sup>+</sup> , [(MIM <sup>+</sup> - H <sub>C2</sub> <sup>+</sup> )CH <sub>2</sub> CHCH <sub>2</sub> NO <sub>2</sub> ] <sup>+</sup> , [(MIM <sup>+</sup> - H <sub>C2</sub> <sup>+</sup> )CH <sub>2</sub> CH(-NO <sub>2</sub> )CH <sub>2</sub> ] <sup>+</sup> , [CH <sub>2</sub> CHCH <sub>2</sub> NC(-ONO)NCN] <sup>+</sup> , [CH <sub>2</sub> CHCH <sub>2</sub> NCNC(-ONO)N] <sup>+</sup> , [MIM <sup>+</sup> CH <sub>2</sub> CHCH <sub>2</sub> ONO] <sup>+</sup> , [MIM <sup>+</sup> CH <sub>2</sub> CH(-ONO)CH <sub>2</sub> ] <sup>+</sup> , [MIM <sup>+</sup> CH <sub>2</sub> CHCH <sub>2</sub> NO <sub>2</sub> ] <sup>+</sup> , <b>MIM<sup>+</sup>CH<sub>2</sub>CH(-NO<sub>2</sub>)CH<sub>2</sub></b>	1592	[CH <sub>2</sub> CHCH <sub>2</sub> NCNC(-ONO)N] <sup>+</sup> , [MIM <sup>+</sup> CH <sub>2</sub> CH(-NO <sub>2</sub> )CH <sub>2</sub> ] <sup>+</sup>
528	CH <sub>2</sub> CHCH <sub>2</sub> DCA, [MIM <sup>+</sup> - H <sub>C2</sub> <sup>+</sup> ]CH <sub>2</sub> CH(-ONO)CH <sub>2</sub> <sup>+</sup> , [CH <sub>2</sub> CHCH <sub>2</sub> NC(-ONO)NCN] <sup>+</sup> , [MIM <sup>+</sup> CH <sub>2</sub> CHCH <sub>2</sub> ONO] <sup>+</sup> , [MIM <sup>+</sup> CH <sub>2</sub> CH(-ONO)CH <sub>2</sub> ] <sup>+</sup> , [MIM <sup>+</sup> CH <sub>2</sub> CH(-NO <sub>2</sub> )CH <sub>2</sub> ] <sup>+</sup>	1456	AIM, [CH <sub>2</sub> CHCH <sub>2</sub> NCNC(-ONO)N] <sup>+</sup>
		1136	[(MIM <sup>+</sup> - H <sub>C2</sub> <sup>+</sup> )CH <sub>2</sub> CHCH <sub>2</sub> ONO] <sup>+</sup> , [CH <sub>2</sub> CHCH <sub>2</sub> NC(-ONO)NCN] <sup>+</sup> , [CH <sub>2</sub> CHCH <sub>2</sub> NCNC(-ONO)N] <sup>+</sup>
		1088	<b>CH<sub>2</sub>=C=CH<sub>2</sub></b> , AIM
		996	AIM, [AMIM <sup>+</sup> - H <sub>C2</sub> <sup>+</sup> - H <sub>ME</sub> ] <sup>+</sup> , [CH <sub>2</sub> CHCH <sub>2</sub> NCNC(-ONO)N] <sup>+</sup> , [MIM <sup>+</sup> CH <sub>2</sub> CHCH <sub>2</sub> ONO] <sup>+</sup> , [MIM <sup>+</sup> CH <sub>2</sub> CHCH <sub>2</sub> NO <sub>2</sub> ] <sup>+</sup> , [MIM <sup>+</sup> CH <sub>2</sub> CH(-NO <sub>2</sub> )CH <sub>2</sub> ] <sup>+</sup>
		919	AIM
		830	[AMIM <sup>+</sup> - H <sub>C2</sub> <sup>+</sup> ], [(MIM <sup>+</sup> - H <sub>C2</sub> <sup>+</sup> )CH <sub>2</sub> CHCH <sub>2</sub> ONO] <sup>+</sup> , [(MIM <sup>+</sup> - H <sub>C2</sub> <sup>+</sup> )CH <sub>2</sub> CH(-ONO)CH <sub>2</sub> ] <sup>+</sup> , [(MIM <sup>+</sup> - H <sub>C2</sub> <sup>+</sup> )CH <sub>2</sub> CHCH <sub>2</sub> NO <sub>2</sub> ] <sup>+</sup> , [(MIM <sup>+</sup> - H <sub>C2</sub> <sup>+</sup> )CH <sub>2</sub> CH(-NO <sub>2</sub> )CH <sub>2</sub> ] <sup>+</sup> , [CH <sub>2</sub> CHCH <sub>2</sub> NCNC(-ONO)N] <sup>+</sup> , [MIM <sup>+</sup> CH <sub>2</sub> CHCH <sub>2</sub> NO <sub>2</sub> ] <sup>+</sup> , [MIM <sup>+</sup> CH <sub>2</sub> CH(-NO <sub>2</sub> )CH <sub>2</sub> ] <sup>+</sup>
		653	[(MIM <sup>+</sup> - H <sub>C2</sub> <sup>+</sup> )CH <sub>2</sub> CHCH <sub>2</sub> ONO] <sup>+</sup>

<sup>a</sup>Ref 12. <sup>b</sup>The species in bold has a dominating IR or Raman intensity at the assigned frequency.

conventional HONO (i.e., the trans-conformer), may also be produced in the experiment.<sup>10</sup> *cis*-HONO has slightly different frequencies than HONO, with the O–N stretch shifting to 1664 cm<sup>-1</sup> and the OH in-plane rocking to 1275 cm<sup>-1</sup>.

The formation of [MIM - H<sub>ME</sub>]<sup>+</sup> (i.e., reaction 3) could be verified by IR peaks at 1481 (ring stretch), 1261 (strong, ring CN stretch and CH rocking), 1039 (ring H–CC–H scissoring), and 781 cm<sup>-1</sup> (strong, ring C–H out-of-plane wagging) and Raman peaks at 1481, 1460 (strong, ring asym N–C–N stretch), 1288 (asym C–N–C stretch), 820 (ring H–CC–H out-of-plane twisting), and 352 cm<sup>-1</sup> (CH<sub>2</sub> wagging).

Reaction of HDCA with NO<sub>2</sub> (i.e., reactions 4a–c) produces another group of products in the experiment. Among these, [HNC(-ONO)NCN]<sup>+</sup> displays strong product-matching IR features at 1397 (CO stretch), 712 (NH out-of-plane rocking), 674 (C–N–C scissoring), and 572 cm<sup>-1</sup> (NO rocking) and Raman features at 2039 (NO stretch), 1996 (strong, asym N–C–N stretch), 1221 (NH in-plane rocking), 988 (asym C–N–C and N–C–N stretch), 470 (DCA out-of-plane twisting), and 461 cm<sup>-1</sup> (DCA in-plane bending). Its decomposition product HNC(O)NCN was identified by its IR peaks at 2243 (asym N–C–N stretch) and 553 cm<sup>-1</sup> (DCA twisting) and Raman peak at 1966 cm<sup>-1</sup> (CO stretch). The formation of [HNCNC(-ONO)N]<sup>+</sup> could be verified by its IR peaks at 1606 (CN

stretch) and 538 cm<sup>-1</sup> (N–C–ONO bending) and Raman peaks at 1845 (NO stretch), 1606, and 1110 cm<sup>-1</sup> (asym N–C–O stretch). The neutral DCA produced from the HT between HDCA and NO<sub>2</sub> shares similar vibrations as its anionic counterpart in BMIM<sup>+</sup>DCA<sup>-</sup>. Its only distinguishable IR and Raman feature is at 1817 cm<sup>-1</sup> (asym DCA stretch).

Reactions of CH<sub>3</sub>DCA and C<sub>4</sub>H<sub>9</sub>DCA with NO<sub>2</sub> lead to the formation of [CH<sub>3</sub>NC(-ONO)NCN]<sup>+</sup>/[C<sub>4</sub>H<sub>9</sub>NC(-ONO)NCN]<sup>+</sup> (reaction 5a) and [CH<sub>3</sub>NCNC(-ONO)N]<sup>+</sup>/[C<sub>4</sub>H<sub>9</sub>NCNC(-ONO)N]<sup>+</sup> (reaction 5b). [CH<sub>3</sub>NC(-ONO)NCN]<sup>+</sup> has product-matching IR peaks at 1371 (CH<sub>3</sub> umbrella), 707 (N–C–N out-of-plane displacement), and 588 cm<sup>-1</sup> (DCA in-plane and out-of-plane bending) and Raman peaks at 2060 (NO stretch), 1371, and 1216 cm<sup>-1</sup> (strong, asym DCA stretch). [C<sub>4</sub>H<sub>9</sub>NC(-ONO)NCN]<sup>+</sup> has similar IR features at 1374 (strong, N–C–O stretch, and CH<sub>2</sub> scissoring), 716 (N–C–N out-of-plane displacement), and 546 cm<sup>-1</sup> (DCA in-plane and out-of-plane bending) and Raman features at 2031 (NO stretch), 1374 (strong), 1135 (strong, CN stretch), and 1108 cm<sup>-1</sup> (CH<sub>2</sub> rocking). The formation of [CH<sub>3</sub>NCNC(-ONO)N]<sup>+</sup> was verified by matching numerous vibrations with the experimentally detected frequencies, including 1801 (strong, CO stretch), 1377 (CH<sub>3</sub> bending), and 578 cm<sup>-1</sup> (N–C–N bending) in infrared, and 2222 (strong, asym N–C–N stretch),

1801, 1601 (CN stretch), 1483 (asym DCA stretch), 1362 (strong, CH<sub>3</sub> umbrella), 1121 (asym N–C–O stretch), and 981 cm<sup>-1</sup> (sym N–C–O stretch) in Raman. Its analogue [C<sub>4</sub>H<sub>9</sub>NCNC(–ONO)N]<sup>•</sup> has distinguishable features at 2181 (strong, asym N–C–N stretch), 1272 (CH<sub>2</sub> wagging), 799 (CN stretch), and 577 cm<sup>-1</sup> (N–C–N bending) in the infrared spectrum and at 1840 (strong, CO stretch), 1363 (CH<sub>2</sub> scissoring), and 497 cm<sup>-1</sup> (N–C–O bending) in Raman.

The reaction of DCA<sup>-</sup> with NO<sub>2</sub> produces [NCNC(–ONO)N]<sup>•-</sup> (reaction 6a) and [NCNCN–NO<sub>2</sub>]<sup>•-</sup> (reaction 6b). They have displayed numerous vibrational peaks for which we are able to find matches in the experimental data. The matching IR peaks are at 2160 (strong, asym N–C–N stretch), 1736 (strong, NO stretch), and 765 cm<sup>-1</sup> (strong, asym skeleton stretch) for [NCNC(–ONO)N]<sup>•-</sup>, and at 2184 (strong, asym N–C–N stretch), 1676 (strong, asym N–C–N stretch), 1533 (strong, O–N–O stretch), 1332 (sym N–C–N and O–N–O stretch), 719 (N–C–N bending), 568 (N–C–N bending and NN stretch), and 559 cm<sup>-1</sup> (N–C–N out-of-plane bending) for [NCNCN–NO<sub>2</sub>]<sup>•-</sup>. The matching Raman peaks are at 1736 cm<sup>-1</sup> for [NCNC(–ONO)N]<sup>•-</sup> and at 1676 (strong), 1533, 1332, 1224 (sym O–N–O stretch), 914 (sym C–N–C stretch), 473 (CC stretch), and 406 cm<sup>-1</sup> (NO<sub>2</sub> rocking) for [NCNCN–NO<sub>2</sub>]<sup>•-</sup>.

Finally, we examined the spectra of [C<sub>2</sub>H<sub>5</sub>CHCH<sub>2</sub>ONO]<sup>•</sup> and [C<sub>2</sub>H<sub>5</sub>CH(–ONO)CH<sub>2</sub>]<sup>•</sup> that are the products of 1-butene with NO<sub>2</sub> (as reaction 7). [C<sub>2</sub>H<sub>5</sub>CHCH<sub>2</sub>ONO]<sup>•</sup> has many vibrations that match the experimental spectra, i.e., IR peaks at 1667 (strong, NO stretch), 1395 (CH<sub>2</sub> scissoring), 1387 (CH<sub>3</sub> bending), 1345 (CC stretch, and CH<sub>2</sub> scissoring and rocking), 1319 (CH<sub>3</sub> umbrella), 1011 (CC stretch), 826 (CH<sub>2</sub> wagging), and 789 cm<sup>-1</sup> (strong, NO stretch) and Raman peaks at 1667, 1356 (CH<sub>2</sub> scissoring), 1345, 1304 (CH<sub>2</sub> wagging), and 654 cm<sup>-1</sup> (N–O–C bending). [C<sub>2</sub>H<sub>5</sub>CH(–ONO)CH<sub>2</sub>]<sup>•</sup>, on the other hand, has only one IR peak at 591 cm<sup>-1</sup> (CO stretch and CH<sub>2</sub> wagging) and two weak Raman peaks at 1366 (CH<sub>2</sub> scissoring) and 633 cm<sup>-1</sup> (CH<sub>2</sub> rocking and NO stretch) that match the experiment, rendering it difficult to confirm its formation in the experiment.

**5.2.2. Product Spectra for AMIM<sup>+</sup>DCA<sup>-</sup> + NO<sub>2</sub>.** The infrared and Raman spectra of the AMIM<sup>+</sup>DCA<sup>-</sup> products share many identical peaks as those of the BMIM<sup>+</sup>DCA<sup>-</sup> products. Table 8 separates the product vibrations of AMIM<sup>+</sup>DCA<sup>-</sup> into two groups: one group consists of the same frequencies as those for BMIM<sup>+</sup>DCA<sup>-</sup> + NO<sub>2</sub> (and thus represent some common products, e.g., neutral DCA, HDCA, CH<sub>3</sub>DCA, [NCNC(–ONO)N]<sup>•-</sup>, [NCNCN–NO<sub>2</sub>]<sup>•-</sup>, [CH<sub>3</sub>NCNC(–ONO)N]<sup>•</sup>, [CH<sub>3</sub>NC(–ONO)NCN]<sup>•</sup>, N<sub>2</sub>O<sub>4</sub>, and HONO), and the other group that was detected only in AMIM<sup>+</sup>DCA<sup>-</sup> + NO<sub>2</sub>.

The intra-ion-pair PT and alkyl abstraction reactions of AMIM<sup>+</sup>DCA<sup>-</sup> produce [AMIM<sup>+</sup> – H<sub>C2</sub><sup>+</sup>], MIM, AIM, CH<sub>2</sub>=C=CH<sub>2</sub>, CH<sub>2</sub>CHCH<sub>2</sub>DCA, CH<sub>3</sub>DCA, and HDCA. MIM, CH<sub>3</sub>DCA, and HDCA are discussed in Section 5.2.1. Herein, we focus on verifying the formation of [AMIM<sup>+</sup> – H<sub>C2</sub><sup>+</sup>], AIM, CH<sub>2</sub>=C=CH<sub>2</sub>, and CH<sub>2</sub>CHCH<sub>2</sub>DCA. [AMIM<sup>+</sup> – H<sub>C2</sub><sup>+</sup>] can be identified by IR peaks at 1342 (CN stretch and CH<sub>3</sub> umbrella), 1279 (asym C–N–C stretch and CH<sub>2</sub> wagging), 1031 (ring H–CC–H scissoring), and 694 cm<sup>-1</sup> (strong, ring H–CC–H out-of-plane wagging) and Raman peaks at 1223 (strong, vinyl CH rocking) and 804 cm<sup>-1</sup> (H–CC–H out-of-plane twisting). CH<sub>2</sub>=C=CH<sub>2</sub> has a distinguishable IR feature at 829 cm<sup>-1</sup> (CH<sub>2</sub> out-of-plane wagging) and Raman peaks at 1954 (asym C–C–C stretch), 1367 (CH<sub>2</sub> bending), and 1053

cm<sup>-1</sup> (strong, sym C–C–C stretch). The product-matching vibrations of CH<sub>2</sub>CHCH<sub>2</sub>DCA include IR peaks at 1533 (strong, sym N–C–N stretch), 1355 (CH<sub>2</sub> bending), 1051 (CH<sub>2</sub> rocking and asym C–C–N stretch), and 548 cm<sup>-1</sup> (CH<sub>2</sub> rocking) and Raman peaks at 2237 (strong, asym N–C–N stretch), 1346 (CH<sub>2</sub> bending), and 1226 cm<sup>-1</sup> (vinyl CH rocking). Identification of AIM was based on its IR peaks at 1357 (CH<sub>2</sub> bending and wagging), 1281 (CH<sub>2</sub> bending and wagging), 804 (ring CH out-of-plane wagging), and 708 cm<sup>-1</sup> (strong, H–CC–H out-of-plane wagging) and Raman peaks at 1470 (ring CC stretch), 1235 (ring and side-chain CN stretch), 1222 (vinyl CH rocking), 1084 (ring CN stretch), 996 (ring C–N–C bending), and 919 cm<sup>-1</sup> (vinyl CH<sub>2</sub> out-of-plane wagging).

The reaction of [AMIM<sup>+</sup> – H<sub>C2</sub><sup>+</sup>] with NO<sub>2</sub> produces [O–AMIM<sup>+</sup> – H<sub>C2</sub><sup>+</sup>] (similar to that in reaction 2a), [AMIM<sup>+</sup> – H<sub>C2</sub><sup>+</sup> – H<sub>ME</sub>]<sup>•</sup> (similar to that in reaction 2b), and [(MIM<sup>+</sup> – H<sub>C2</sub><sup>+</sup>)CH<sub>2</sub>CHCH<sub>2</sub>ONO]<sup>•</sup>, [(MIM<sup>+</sup> – H<sub>C2</sub><sup>+</sup>)CH<sub>2</sub>CH(–ONO)CH<sub>2</sub>]<sup>•</sup>, [(MIM<sup>+</sup> – H<sub>C2</sub><sup>+</sup>)CH<sub>2</sub>CHCH<sub>2</sub>NO<sub>2</sub>]<sup>•</sup>, and [(MIM<sup>+</sup> – H<sub>C2</sub><sup>+</sup>)CH<sub>2</sub>CH(–NO<sub>2</sub>)CH<sub>2</sub>]<sup>•</sup>, which are due to the reactions of the allyl group with NO<sub>2</sub>. Formation of [O–AMIM<sup>+</sup> – H<sub>C2</sub><sup>+</sup>] can be verified by its strong characteristic IR peak at 1665 cm<sup>-1</sup> (CO stretch) and others at 1351 (CH<sub>2</sub> bending) and 1268 cm<sup>-1</sup> (CH rocking). Formation of [AMIM<sup>+</sup> – H<sub>C2</sub><sup>+</sup> – H<sub>ME</sub>]<sup>•</sup> is consistent with the observation of its IR peaks at 1373 (CH<sub>2</sub> bending), 1347 (CH<sub>2</sub> bending), 1033 (H–CC–H scissoring), and 696 cm<sup>-1</sup> (ring N–C–N bending) and Raman peaks at 1241 (asym ring C–N–C stretch), 1221 (vinyl CH rocking), and 994 cm<sup>-1</sup> (ring CN stretch and vinyl CH<sub>2</sub> rocking). [(MIM<sup>+</sup> – H<sub>C2</sub><sup>+</sup>)CH<sub>2</sub>CHCH<sub>2</sub>ONO]<sup>•</sup> shows many product-matching features. The ones of significant intensities are 1682 (NO stretch), 1345 (CH<sub>2</sub> bending and CH<sub>3</sub> umbrella), 1047 (CH<sub>2</sub> rocking and CCC bending), and 689 cm<sup>-1</sup> (ring H–CC–H out-of-plane wagging) in its IR spectrum and 1682, 1118 (CH<sub>2</sub> twisting), 800 (ring H–CC–H out-of-plane twisting), and 632 cm<sup>-1</sup> (sym C–O–N stretch) in its Raman spectra. The vibrational spectra of [(MIM<sup>+</sup> – H<sub>C2</sub><sup>+</sup>)CH<sub>2</sub>CH(–ONO)CH<sub>2</sub>]<sup>•</sup> are similar to those of [(MIM<sup>+</sup> – H<sub>C2</sub><sup>+</sup>)CH<sub>2</sub>CHCH<sub>2</sub>ONO]<sup>•</sup>, and its product-matching IR peaks are at 1684 (strong, NO stretch), 1348 (CH<sub>2</sub> bending and CH<sub>3</sub> umbrella), 1262 (CH<sub>2</sub> wagging), 1060 (CH<sub>2</sub> rocking), 1041 (ring H–CC–H scissoring), and 507 cm<sup>-1</sup> (strong, CH<sub>2</sub> wagging) and Raman peaks at 1684, 1339 (sym ring stretch), and 800 cm<sup>-1</sup> (ring H–CC–H out-of-plane twisting). The product-matching spectral features of [(MIM<sup>+</sup> – H<sub>C2</sub><sup>+</sup>)CH<sub>2</sub>CHCH<sub>2</sub>NO<sub>2</sub>]<sup>•</sup> include IR peaks at 1347 (CH<sub>3</sub> umbrella and CN stretch), 1031 (ring H–CC–H scissoring), and 699 cm<sup>-1</sup> (strong, ring H–CC–H out-of-plane wagging) and Raman peaks at 1347, 1229 (CH<sub>2</sub> wagging), and 841 cm<sup>-1</sup> (O–N–O bending and CN stretch). [(MIM<sup>+</sup> – H<sub>C2</sub><sup>+</sup>)CH<sub>2</sub>CH(–NO<sub>2</sub>)CH<sub>2</sub>]<sup>•</sup> has similar characteristic peaks as [(MIM<sup>+</sup> – H<sub>C2</sub><sup>+</sup>)CH<sub>2</sub>CHCH<sub>2</sub>NO<sub>2</sub>]<sup>•</sup>, including IR peaks at 1348 (CH<sub>3</sub> umbrella and CN stretch), 1034 (ring H–CC–H scissoring), 827 (O–N–O bending and CN stretch), and 693 cm<sup>-1</sup> (strong, ring H–CC–H out-of-plane wagging) and Raman peaks at 1338 (sym ring stretch), 827, and 488 cm<sup>-1</sup> (CH<sub>2</sub> wagging).

Reaction of CH<sub>2</sub>CHCH<sub>2</sub>DCA with NO<sub>2</sub> results in [CH<sub>2</sub>CHCH<sub>2</sub>NC(–ONO)NCN]<sup>•</sup> (reaction 5a) and [CH<sub>2</sub>CHCH<sub>2</sub>NCNC(–ONO)N]<sup>•</sup> (reaction 5b). Despite that [CH<sub>2</sub>CHCH<sub>2</sub>NC(–ONO)NCN]<sup>•</sup> presents many IR peaks that match the experimental spectra, its most intense peak at 2073 cm<sup>-1</sup> was not detected in the experiment, making the formation of this product doubtful. [CH<sub>2</sub>CHCH<sub>2</sub>NCNC(–ONO)N]<sup>•</sup>, on the other hand, has all vibrational peaks that are able to match

either reactant or product spectra. Its infrared peaks at 1702 (strong, CO stretch), 808 (CN stretch and CH<sub>2</sub> rocking), and 728 cm<sup>-1</sup> (strong, NCN bending) and Raman peaks at 1364 (CH<sub>2</sub> bending), 1224 (vinyl CH rocking), 1107 (asym O–C–N stretch), 981 (vinyl CH<sub>2</sub> twisting), and 808 cm<sup>-1</sup> are close to the product spectra. The formation of [CH<sub>2</sub>C(–ONO)CH<sub>2</sub>]<sup>•</sup> from the reaction of allene with NO<sub>2</sub> was confirmed by the observation of its IR peaks at 1694 cm<sup>-1</sup> (strong, CO stretch) and the Raman peaks at 1227 (C–C–C bending) and 477 cm<sup>-1</sup> (CO stretch and allyl rocking).

Besides the fact that AMIM<sup>+</sup>DCA<sup>-</sup> has followed similar routes of reactions 1–7 as EMIM<sup>+</sup>DCA<sup>-</sup> and BMIM<sup>+</sup>DCA<sup>-</sup>, the allyl group of AMIM<sup>+</sup> reacts with NO<sub>2</sub> and produces [MIM<sup>+</sup>CH<sub>2</sub>CHCH<sub>2</sub>ONO]<sup>•</sup>, [MIM<sup>+</sup>CH<sub>2</sub>CH(–ONO)CH<sub>2</sub>]<sup>•</sup>, [MIM<sup>+</sup>CH<sub>2</sub>CHCH<sub>2</sub>NO<sub>2</sub>]<sup>•</sup>, and [MIM<sup>+</sup>CH<sub>2</sub>CH(–NO<sub>2</sub>)–CH<sub>2</sub>]<sup>•</sup>. As shown in Figure 11 and Table 8, the four adducts demonstrate similar product-matching infrared features. Their infrared vibrations at 1700 cm<sup>-1</sup> correspond to CO stretch, 1520 cm<sup>-1</sup> to asym N–C–N and/or O–N–N stretch, 1360 cm<sup>-1</sup> to CH<sub>2</sub>/CH<sub>3</sub> bending, 1240 cm<sup>-1</sup> to CH<sub>2</sub> wagging, 1050 cm<sup>-1</sup> to CH<sub>2</sub> rocking and ring CH wagging, 845 cm<sup>-1</sup> to O–N–O bending, 820 and 710 cm<sup>-1</sup> to ring CH out-of-plane rocking, and 510 cm<sup>-1</sup> to CH<sub>2</sub> rocking and/or O–C–C bending. The four adducts also present product-matching Raman peaks but with very low intensities.

## 6. CONCLUSIONS

Direct dynamics trajectories were used to find the most likely reaction pathways and products for the NO<sub>2</sub> oxidation of EMIM<sup>+</sup>DCA<sup>-</sup>, BMIM<sup>+</sup>DCA<sup>-</sup>, and AMIM<sup>+</sup>DCA<sup>-</sup>. Analysis of the trajectory outcomes combined with the calculations of reaction coordinates and reaction energetics for the trajectory-predicted pathways revealed intra-ion-pair proton transfer and alkyl abstraction in 1,3-dialkylimidazolium–DCA as the two dominant primary processes followed by the secondary reactions of the proton-transferred products (including [dialkylimidazolium<sup>+</sup> – H<sub>2</sub>C<sup>+</sup>], MIM, HDCA, C<sub>2</sub>H<sub>4</sub>, 1-C<sub>4</sub>H<sub>8</sub>, and CH<sub>2</sub>=C=CH<sub>2</sub>) and the alkyl-abstracted products (including MIM, EIM, BIM, AIM, and alkyl-DCA) with NO<sub>2</sub>. The good match between the theoretically predicted and experimentally measured reactivities of BMIM<sup>+</sup>DCA<sup>-</sup> and AMIM<sup>+</sup>DCA<sup>-</sup> toward NO<sub>2</sub> and between the simulated and the measured vibrational spectra of oxidation products suggests that our computational modeling has captured the important IL oxidation dynamics.

The main differences among the three dialkylimidazolium–DCA ILs are the statistical factor for intra-ion-pair H<sup>β</sup>-proton transfer (three for EMIM<sup>+</sup>DCA<sup>-</sup>, followed by two for BMIM<sup>+</sup>DCA<sup>-</sup> and then one for AMIM<sup>+</sup>DCA<sup>-</sup>) and the accompanying alkene elimination, and that only the reaction of AMIM<sup>+</sup>DCA<sup>-</sup> is endoergic. These facts account for the relatively low reactivity of AMIM<sup>+</sup>DCA<sup>-</sup>. It is interesting to compare the results of dialkylimidazolium–DCA + NO<sub>2</sub> with that of MAT<sup>+</sup>DCA<sup>-</sup> + NO<sub>2</sub>. The differences between the NO<sub>2</sub> oxidation reactions of EMIM<sup>+</sup>DCA<sup>-</sup>, BMIM<sup>+</sup>DCA<sup>-</sup>, AMIM<sup>+</sup>DCA<sup>-</sup>, and MAT<sup>+</sup>DCA<sup>-</sup> are resulting from the different cation structures of the dialkylimidazolium and the alkyltriazolium, while their similarities are associated with the reactions of the same DCA<sup>-</sup> anion and the HDCA product molecule. When comparing the product spectra of BMIM<sup>+</sup>DCA<sup>-</sup> and AMIM<sup>+</sup>DCA<sup>-</sup> + NO<sub>2</sub> vs MAT<sup>+</sup>DCA<sup>-</sup> + NO<sub>2</sub>,<sup>10</sup> we indeed found many common vibrations, including the IR peaks at 2260–2170, 1524–1497, 1373–1356, and 1040 cm<sup>-1</sup> and the

Raman peaks at 2020–2010, 1867–1868, 497–492, and 416–409 cm<sup>-1</sup>. The fact that all of the common vibrational peaks can match the reaction products of HDCA + NO<sub>2</sub> and DCA<sup>-</sup> + NO<sub>2</sub> supports our interpretation. The experimental results indicate that the reaction rate constant of MAT<sup>+</sup>DCA<sup>-</sup> is a factor of 20 lower than that of BMIM<sup>+</sup>DCA<sup>-</sup>. The extremely low reactivity of MAT<sup>+</sup>DCA<sup>-</sup> is mainly due to the lack of H<sup>β</sup>-transfer and alkyl abstraction, whereas both of these reactions are exoergic in the case of dialkylimidazolium–DCA and, respectively, produce alkene and alkyl-DCA, releasing energy that promotes further reactions in the dialkylimidazolium–DCA ILs.

The trajectories and the analysis of reaction energetics have supported that the DCA-based ILs are not hypergolic with NO<sub>2</sub>. In fact, the addition of N<sub>2</sub>O<sub>4</sub>/NO<sub>2</sub> has made the ignition delay time longer in the hypergolic reaction of BMIM<sup>+</sup>DCA<sup>-</sup> with HNO<sub>3</sub>.<sup>55</sup> However, NO<sub>2</sub> is indeed produced in the hypergolic reactions via the thermal decomposition of HNO<sub>3</sub>.<sup>56</sup> In this context, the work on the NO<sub>2</sub> oxidation of dialkylimidazolium–DCA ILs provides insights into the IL oxidation and combustion chemistry that occur at high temperatures.

## ■ ASSOCIATED CONTENT

### Supporting Information

The Supporting Information is available free of charge at <https://pubs.acs.org/doi/10.1021/acs.jpbc.0c02253>.

Computational methods, reactions of NO<sub>2</sub> with HDCA and DCA<sup>-</sup>, infrared and Raman spectra of BMIM<sup>+</sup>DCA<sup>-</sup> and AMIM<sup>+</sup>DCA<sup>-</sup>, and Cartesian coordinates for the calculated structures (PDF)

Video for the trajectory is shown in Figure 1 (MPG)

## ■ AUTHOR INFORMATION

### Corresponding Author

Jianbo Liu – Department of Chemistry and Biochemistry, Queens College and the Graduate Center of the City University of New York, Queens, New York 11367, United States; [orcid.org/0000-0001-9577-3740](https://orcid.org/0000-0001-9577-3740); Phone: 1-718-997-3271; Email: [jianbo.liu@qc.cuny.edu](mailto:jianbo.liu@qc.cuny.edu)

### Authors

Wenjing Zhou – Department of Chemistry and Biochemistry, Queens College and the Graduate Center of the City University of New York, Queens, New York 11367, United States

Steven D. Chambreau – ERC, Inc., Air Force Research Laboratory, Edwards Air Force Base, California 93524, United States

Ghanshyam L. Vaghjiani – In-Space Propulsion Branch, Rocket Propulsion Division, Aerospace Systems Directorate, Air Force Research Laboratory, AFRL/RQRS, Edwards Air Force Base, California 93524, United States; [orcid.org/0000-0001-7473-7388](https://orcid.org/0000-0001-7473-7388)

Complete contact information is available at: <https://pubs.acs.org/10.1021/acs.jpbc.0c02253>

### Notes

The authors declare no competing financial interest.

## ■ ACKNOWLEDGMENTS

J.L. acknowledges the support from the AFRL through ERC Contract no. PS170079 and the Air Force Office of Scientific Research under Contract no. FA 9300-06-C-0023. The authors

acknowledge Dr. Jerry Boatz (AFRL/RQRP) for valuable discussions regarding quantum chemistry approaches.

## REFERENCES

- (1) Zhang, Q.; Shreeve, J. M. Energetic Ionic Liquids as Explosives and Propellant Fuels: A New Journey of Ionic Liquid Chemistry. *Chem. Rev.* **2014**, *114*, 10527–10574.
- (2) Smiglak, M.; Metlen, A.; Rogers, R. D. The Second Evolution of Ionic Liquids: From Solvents and Separations to Advanced Materials-Energetic Examples from the Ionic Liquid Cookbook. *Acc. Chem. Res.* **2007**, *40*, 1182–1192.
- (3) McCrary, P. D.; Chatel, G.; Alaniz, S. A.; Cojocar, O. A.; Beasley, P. A.; Flores, L. A.; Kelley, S. P.; Barber, P. S.; Rogers, R. D. Evaluating Ionic Liquids as Hypergolic Fuels: Exploring Reactivity from Molecular Structure. *Energy Fuels* **2014**, *28*, 3460–3473.
- (4) Schneider, S.; Hawkins, T.; Rosander, M.; Mills, J.; Vaghjiani, G.; Chambreau, S. Liquid Azide Salts and Their Reactions with Common Oxidizers Iridium and  $N_2O_4$ . *Inorg. Chem.* **2008**, *47*, 6082–6089.
- (5) Schneider, S.; Hawkins, T.; Rosander, M.; Vaghjiani, G.; Chambreau, S.; Drake, G. Ionic Liquids as Hypergolic Fuels. *Energy Fuels* **2008**, *22*, 2871–2872.
- (6) Catoire, L.; Chambreau, S. D.; Vaghjiani, G. L. Chemical Kinetics Interpretation of Hypergolicity of Dicyanamide Ionic Liquid-Based Systems. *Combust. Flame* **2012**, *159*, 1759–1768.
- (7) Chambreau, S. D.; Schenk, A. C.; Sheppard, A. J.; Yandek, G. R.; Vaghjiani, G. L.; Maciejewski, J.; Koh, C. J.; Golan, A.; Leone, S. R. Thermal Decomposition Mechanisms of Alkylimidazolium Ionic Liquids with Cyano-Containing Anions. *J. Phys. Chem. A* **2014**, *118*, 11119–11132.
- (8) Liu, J.; Chambreau, S. D.; Vaghjiani, G. L. Dynamics Simulations and Statistical Modeling of Thermal Decomposition of 1-Ethyl-3-Methylimidazolium Dicyanamide and 1-Ethyl-2,3-Dimethylimidazolium Dicyanamide. *J. Phys. Chem. A* **2014**, *118*, 11133–11144.
- (9) Brotton, S. J.; Lucas, M.; Chambreau, S. D.; Vaghjiani, G. L.; Yu, J.; Anderson, S. L.; Kaiser, R. I. Spectroscopic Investigation of the Primary Reaction Intermediates in the Oxidation of Levitated Droplets of Energetic Ionic Liquids. *J. Phys. Chem. Lett.* **2017**, *8*, 6053–6059.
- (10) Liu, J.; Zhou, W.; Chambreau, S. D.; Vaghjiani, G. L. Computational Study of the Reaction of 1-Methyl-4-Amino-1,2,4-Triazolium Dicyanamide with  $NO_2$ : From Reaction Dynamics to Potential Surfaces, Kinetics and Spectroscopy. *J. Phys. Chem. B* **2019**, *123*, 2956–2970.
- (11) Brotton, S. J.; Lucas, M.; Jensen, T. N.; Anderson, S. L.; Kaiser, R. I. Spectroscopic Study on the Intermediates and Reaction Rates in the Oxidation of Levitated Droplets of Energetic Ionic Liquids by Nitrogen Dioxide. *J. Phys. Chem. A* **2018**, *122*, 7351–7377.
- (12) Lucas, M.; Brotton, S. J.; Shukla, S. K.; Yu, J.; Anderson, S. L.; Kaiser, R. I. Oxidation of a Levitated Droplet of 1-Allyl-3-methylimidazolium Dicyanamide by Nitrogen Dioxide. *J. Phys. Chem. A* **2019**, *123*, 400–416.
- (13) Chowdhury, A.; Thynell, S. T. Confined Rapid Thermolysis/FTIR/ToF Studies of Imidazolium-Based Ionic Liquids. *Thermochim. Acta* **2006**, *443*, 159–172.
- (14) Marcus, R. A. Unimolecular Dissociations and Free-Radical Recombination Reactions. *J. Chem. Phys.* **1952**, *20*, 359–364.
- (15) Car, R.; Parrinello, M. Unified Approach for Molecular Dynamics and Density Functional Theory. *Phys. Rev. Lett.* **1985**, *55*, 2471–2474.
- (16) Baldridge, K. K.; Gordon, M. S.; Steckler, R.; Truhlar, D. G. Ab Initio Reaction Paths and Direct Dynamics Calculations. *J. Phys. Chem. A* **1989**, *93*, 5107–5119.
- (17) Helgaker, T.; Uggerud, E.; Jensen, H. J. A. Integration of the Classical Equations of Motion on Ab Initio Molecular Potential Energy Surfaces Using Gradients and Hessians: Application to Translational Energy Release Upon Fragmentation. *Chem. Phys. Lett.* **1990**, *173*, 145–150.
- (18) Bolton, K.; Hase, W. L.; Peslherbe, G. H. Direct Dynamics Simulations of Reactive Systems. In *Modern Methods for Multidimensional Dynamics Computations in Chemistry*; Thompson, D. L., Ed.; World Scientific: Singapore, 1998; pp 143–189.
- (19) Hase, W. L. Advances in Classical Trajectory Methods. *Intramolecular and Nonlinear Dynamics*; JAI: Greenwich, Connecticut, 1992; Vol 1, p 399.
- (20) Bakken, V.; Millam, J. M.; Schlegel, H. B. Ab Initio Classical Trajectories on the Born-Oppenheimer Surface: Updating Methods for Hessian-Based Integrators. *J. Chem. Phys.* **1999**, *111*, 8773–8777.
- (21) Döntgen, M.; Przybylski-Freund, M.-D.; Kröger, L. C.; Kopp, W. A.; Ismail, A. E.; Leonhard, K. Automated Discovery of Reaction Pathways, Rate Constants, and Transition States Using Reactive Molecular Dynamics Simulations. *J. Chem. Theory Comput.* **2015**, *11*, 2517–2524.
- (22) Martínez-Núñez, E. An Automated Transition State Search Using Classical Trajectories Initialized at Multiple Minima. *Phys. Chem. Chem. Phys.* **2015**, *17*, 14912–14921.
- (23) Pratihari, S.; Ma, X.; Homayoon, Z.; Barnes, G. L.; Hase, W. L. Direct Chemical Dynamics Simulations. *J. Am. Chem. Soc.* **2017**, *139*, 3570–3590.
- (24) Ma, X.; Hase, W. L. Perspective: Chemical Dynamics Simulations of Non-Statistical Reaction Dynamics. *Philos. Trans. R. Soc. A* **2017**, *375*, No. 20160204.
- (25) Sun, R.; Siebert, M. R.; Xu, L.; Chambreau, S. D.; Vaghjiani, G. L.; Lischka, H.; Liu, J.; Hase, W. L. Direct Dynamics Simulation of the Activation and Dissociation of 1,5-Dinitrobiuret (HDNB). *J. Phys. Chem. A* **2014**, *118*, 2228–2236.
- (26) Martínez-Núñez, E. An Automated Method to Find Transition States Using Chemical Dynamics Simulations. *J. Comput. Chem.* **2015**, *36*, 222–234.
- (27) Hase, W. L.; Bolton, K.; de Sainte Claire, P.; Duchovic, R. J.; Hu, X.; Komornicki, A.; Li, G.; Lim, K.; Lu, D.; Peslherbe, G. H.; Song, K.; Swamy, K. N.; Vande Linde, S. R.; Varandas, A.; Wang, H.; Wolf, R. J. *Venus 99: A General Chemical Dynamics Computer Program*; Texas Tech University: Lubbock, TX, 1999.
- (28) Hu, X.; Hase, W. L.; Pirraglia, T. Vectorization of the General Monte Carlo Classical Trajectory Program Venus. *J. Comput. Chem.* **1991**, *12*, 1014–1024.
- (29) Frisch, M. J.; Trucks, G. W.; Schlegel, H. B.; Scuseria, G. E.; Robb, M. A.; Cheeseman, J. R.; Scalmani, G.; Barone, V.; Mennucci, B.; Petersson, G. A. et al. *Gaussian 09*, revision B.01; Gaussian, Inc., 2009.
- (30) Kroon, M. C.; Buijs, W.; Peters, C. J.; Witkamp, G.-J. Quantum Chemical Aided Prediction of the Thermal Decomposition Mechanisms and Temperatures of Ionic Liquids. *Thermochim. Acta* **2007**, *465*, 40–47.
- (31) Emel'yanenko, V. N.; Verevkin, S. P.; Heintz, A. The Gaseous Enthalpy of Formation of the Ionic Liquid 1-Butyl-3-methylimidazolium Dicyanamide from Combustion Calorimetry, Vapor Pressure Measurements, and Ab Initio Calculations. *J. Am. Chem. Soc.* **2007**, *129*, 3930–3937.
- (32) Verevkin, S. P.; Emel'yanenko, V. N.; Zaitsau, D. H.; Heintz, A.; Muzny, C. D.; Frenkel, M. Thermochemistry of Imidazolium-Based Ionic Liquids: Experiment and First-Principles Calculations. *Phys. Chem. Chem. Phys.* **2010**, *12*, 14994–15000.
- (33) Hollóczki, O.; Gerhard, D.; Massone, K.; Szarvas, L.; Németh, B.; Veszprémi, T.; Nyulászi, L. Carbenes in Ionic Liquids. *New J. Chem.* **2010**, *34*, 3004–3009.
- (34) Clough, M. T.; Geyer, K.; Hunt, P. A.; Mertes, J.; Welton, T. Thermal Decomposition of Carboxylate Ionic Liquids: Trends and Mechanisms. *Phys. Chem. Chem. Phys.* **2013**, *15*, 20480–20495.
- (35) Gao, Y.; Gao, H.; Piekarski, C.; Shreeve, J. M. Azolium Salts Functionalized with Cyanomethyl, Vinyl, or Propargyl Substituents and Dicyanamide, Dinitramide, Perchlorate and Nitrate Anions. *Eur. J. Inorg. Chem.* **2007**, *2007*, 4965–4972.
- (36) Talaty, E. R.; Raja, S.; Storhaug, V. J.; Doelle, A.; Carper, W. R. Raman and Infrared Spectra and Ab Initio Calculations of  $C_{2-4}$ MIM Imidazolium Hexafluorophosphate Ionic Liquids. *J. Phys. Chem. B* **2004**, *108*, 13177–13184.
- (37) Heimer, N. E.; Del Sesto, R. E.; Meng, Z.; Wilkes, J. S.; Carper, W. R. Vibrational Spectra of Imidazolium Tetrafluoroborate Ionic Liquids. *J. Mol. Liq.* **2006**, *124*, 84–95.

- (38) Katsyuba, S. A.; Zvereva, E. E.; Vidis, A.; Dyson, P. J. Application of Density Functional Theory and Vibrational Spectroscopy toward the Rational Design of Ionic Liquids. *J. Phys. Chem. A* **2007**, *111*, 352–370.
- (39) Holomb, R.; Martinelli, A.; Albinsson, I.; Lassegues, J. C.; Johansson, P.; Jacobsson, P. Ionic Liquid Structure: The Conformational Isomerism in 1-Butyl-3-Methylimidazolium Tetrafluoroborate ([BMIM][BF<sub>4</sub>]). *J. Raman Spectrosc.* **2008**, *39*, 793–805.
- (40) Xuan, X.-P.; Guo, M.; Pei, Y.-C.; Zheng, Y. Theoretical Study on Cation-Anion Interaction and Vibrational Spectra of 1-Allyl-3-Methylimidazolium-Based Ionic Liquids. *Spectrochim. Acta, Part A* **2011**, *78*, 1492–1499.
- (41) Bacskay, G. B. A Quadratically Convergent Hartree-Fock (QC-SCF) Method. Application to Closed Shell Systems. *Chem. Phys.* **1981**, *61*, 385–404.
- (42) Laaksonen, L. *gOpenMol*, version 3.0; Center for Scientific Computing: Espoo, Finland, 2005.
- (43) Frisch, M. J.; Trucks, G. W.; Schlegel, H. B.; Scuseria, G. E.; Robb, M. A.; Cheeseman, J. R.; Scalmani, G.; Barone, V.; Petersson, G. A.; Nakatsuji, H. et al. *Gaussian 16*, revision B.01; Gaussian, Inc.: Wallingford, CT, 2016.
- (44) Alecu, I. M.; Zheng, J.; Zhao, Y.; Truhlar, D. G. Computational Thermochemistry: Scale Factor Databases and Scale Factors for Vibrational Frequencies Obtained from Electronic Model Chemistries. *J. Chem. Theory Comput.* **2010**, *6*, 2872–2887.
- (45) Marenich, A. V.; Cramer, C. J.; Truhlar, D. G. Universal Solvation Model Based on Solute Electron Density and on a Continuum Model of the Solvent Defined by the Bulk Dielectric Constant and Atomic Surface Tensions. *J. Phys. Chem. B* **2009**, *113*, 6378–6396.
- (46) Bernales, V. S.; Marenich, A. V.; Contreras, R.; Cramer, C. J.; Truhlar, D. G. Quantum Mechanical Continuum Solvation Models for Ionic Liquids. *J. Phys. Chem. B* **2012**, *116*, 9122–9129.
- (47) Zhao, Y.; Truhlar, D. G. Density Functionals with Broad Applicability in Chemistry. *Acc. Chem. Res.* **2008**, *41*, 157–167.
- (48) Chambreau, S. D.; Boatz, J. A.; Vaghjiani, G. L.; Koh, C.; Kostko, O.; Golan, A.; Leone, S. R. Thermal Decomposition Mechanism of 1-Ethyl-3-methylimidazolium Bromide Ionic Liquid. *J. Phys. Chem. A* **2012**, *116*, 5867–5876.
- (49) Sprung, J. L.; Akimoto, H.; Pitts, J. N., Jr. Nitrogen Dioxide Catalyzed Geometric Isomerization of Olefins. Isomerization Kinetics of the 2-Butenes and 2-Pentenes. *J. Am. Chem. Soc.* **1974**, *96*, 6549–6554.
- (50) Park, J. S. B.; Walton, J. C. Reactions of Nitric Oxide and Nitrogen Dioxide with Functionalized Alkenes and Dienes. *J. Chem. Soc., Perkin Trans. 2* **1997**, *12*, 2579–2583.
- (51) Giménez-López, J.; Alzueta, M. U.; Rasmussen, C. T.; Marshall, P.; Glarborg, P. High Pressure Oxidation of C<sub>2</sub>H<sub>4</sub>/NO Mixtures. *Proc. Combust. Inst.* **2011**, *33*, 449–457.
- (52) Deng, F.; Zhang, Y.; Sun, W.; Huang, W.; Zhao, Q.; Qin, X.; Yang, F.; Huang, Z. Towards a Kinetic Understanding of the NO<sub>x</sub> Sensitization Effect on Unsaturation Hydrocarbons: A Case Study of Ethylene/Nitrogen Dioxide Mixtures. *Proc. Combust. Inst.* **2019**, *37*, 719–726.
- (53) Truhlar, D. G.; Garrett, B. C.; Klippenstein, S. J. Current Status of Transition-State Theory. *J. Phys. Chem. B* **1996**, *100*, 12771–12800.
- (54) Herzberg, G. *Molecular Spectra and Molecular Structure. I. Diatomic Molecules*, 2th ed.; Krieger Publishing Company: Malabar, Florida, 1950; p 660.
- (55) Chambreau, S. D.; Koh, C. J.; Popolan-Vaida, D. M.; Gallegos, C. J.; Hooper, J. B.; Bedrov, D.; Vaghjiani, G. L.; Leone, S. R. Flow-Tube Investigations of Hypergolic Reactions of a Dicyanamide Ionic Liquid Via Tunable Vacuum Ultraviolet Aerosol Mass Spectrometry. *J. Phys. Chem. A* **2016**, *120*, 8011–8023.
- (56) Thomas, A. E.; Chambreau, S. D.; Redeker, N. D.; Esparza, A. A.; Shafirovich, E.; Ribbeck, T.; Sprenger, J. A. P.; Finze, M.; Vaghjiani, G. L. Thermal Decomposition and Hypergolic Reaction of a Dicyanoborohydride Ionic Liquid. *J. Phys. Chem. A* **2020**, *124*, 864–874.